Sulfate attack on structural concretes: from microscopic mechanisms to engineering modeling

> fib Symposium 2025, Antibes, France <

Prof. Kefei Li, Tsinghua University, Beijing, China

June 16, 2025

清華大學土木水利学院
SCHOOL OF CIVIL ENGINEERING
TSINGHUA UNIVERSITY

Lecture outline

1 Background (State-of-the-art & Challenges)

2 Sulfate attack (AFt formation, expansion & poromechanics)

3 Spalling rate (modeling, validation & applications)

4 Concluding remarks (conclusions & perspectives)

1 Background. Sulfate attack

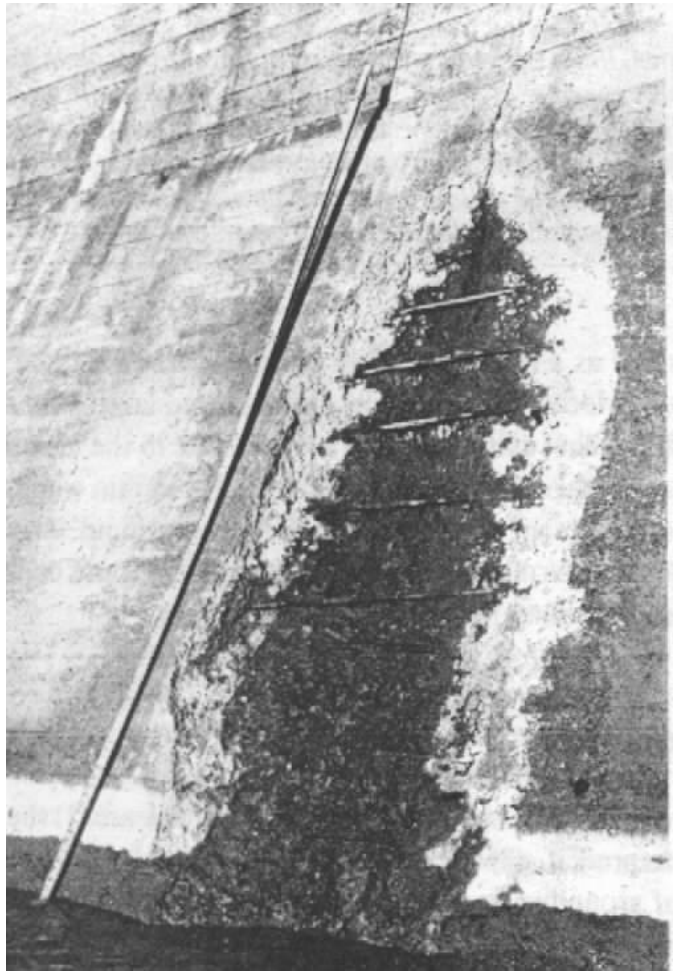

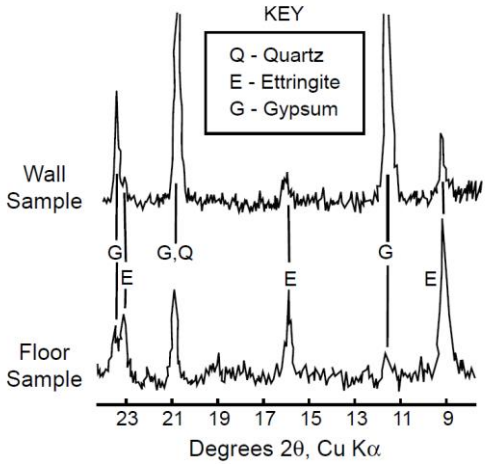

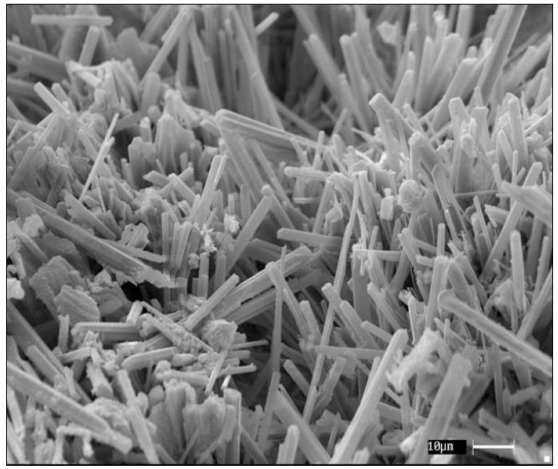

Figure Sulphate attack on concrete in Fort Peck Dam ,1971. The sulphate concentration in the groundwater is 10,000 mg/L and Type I Portland cement was used with 0.49 water to cement ratio and 7-9% C_3A content in cement. Source: Figure 5-17 in (Mehta and Monterio, 2006)

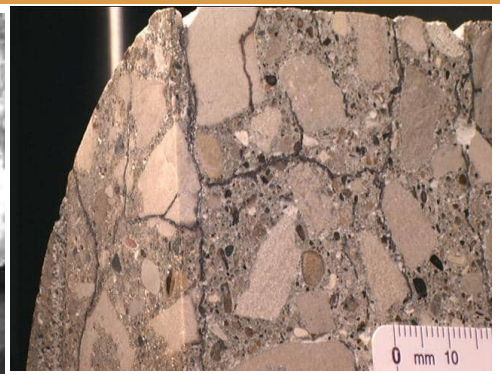

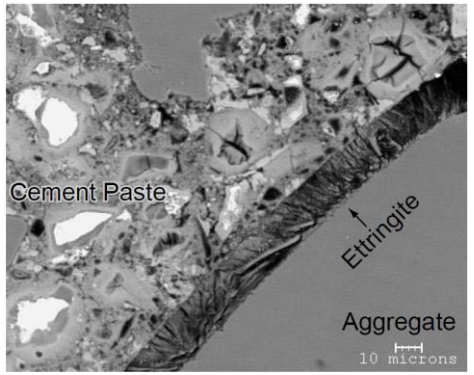

Figure The concrete elements without direct contact with the external sulphate source can also have ettringite formed after hardening, i.e. delayed ettringite formation (DEF), which is caused by the high temperature curing (above 65°C) and the sulphates absorbed by CSH.

Source: https://civildigital.com/significance-delayed-ettringite-formation-damage-mechanisms/image189/

1 Background. Challenges

"Sulfate attack on concrete structures in service is not widespread except in some areas, and the amount of **laboratory-based research** seems to be **disproportionately large**. On the other hand, our **knowledge** and understanding of sulfate attack **in the field** remains **inadequate**."

---*from* Adam Naville, The confused world of sulfate attack on concrete, Cement and Concrete Research 34(2004) 1275-1296

Fill in the gap ...

Aerial View of the Great Rift Valley of Eastern Africa. Philippe Bourseiller / Getty Images, source: https://www.thoughtco.com/what-is-the-rift-valley-172559

Sulfate attack in field occurs along with other agents or processes such as chlorides, leaching process etc.

(Reaction scale)

(Pore scale)

Sulfate attack damages concrete materials through the pore crystallization and the related stress, thus poromechanics of crystallization is needed.

(Structural scale)

Sulfate attack damage need to be described & addressed on the structural level, thus pertinent damage model on structural level is needed.

2 Sulfate attack

Source: https://www.thoughtco.com/definition-of-crystallize-605854

Crystallization

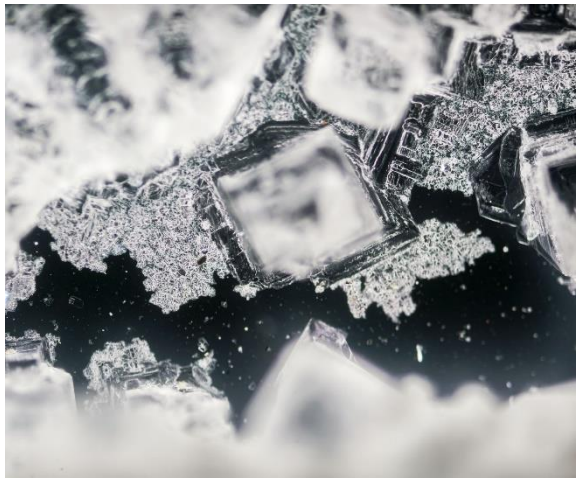

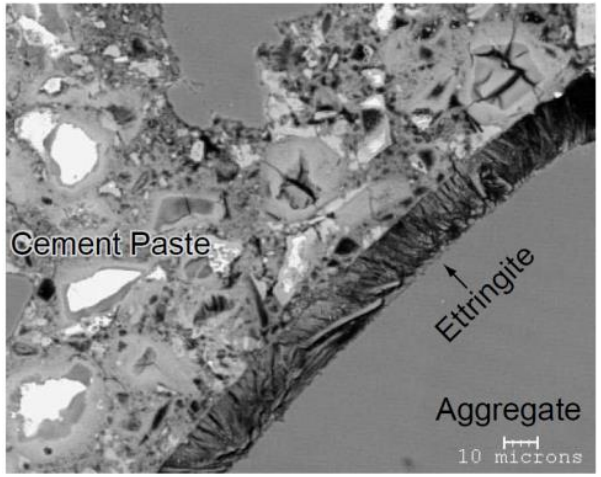

Expansion

Source: Figure 5-15 from (Mehta and Monterio, 2006)

2 Sulfate attack. Experiments

清華大学土木水利学院
SCHOOL OF CIVIL ENGINEERING
TSINGHUA UNIVERSITY

Cement paste using CEM I 52.5R cement, w/c of 0.55, cured for 60d in saturated CH solution

Slice specimens 2mm*4cm*4cm

Slice specimens 2mm*2cm*12cm

Investigate:

☞ AFt formation/Pore structure

☞ Diffusivity/Expansion

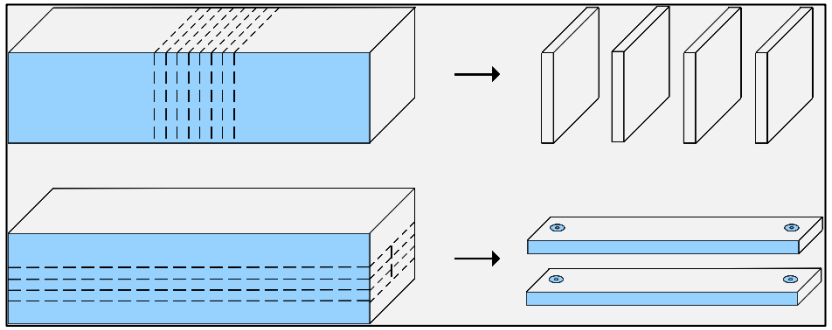

Table 2
Composition of sulfate and mixed solutions.

Notation	SO_4^{2-} concentration	Cl^- concentration	OH^- concentration	Na^+ concentration
C1	10 g/L	0	0.1 mol/L	0.308 mol/L
C2	10 g/L	10 g/L	0.1 mol/L	0.590 mol/L
C3	10 g/L	19 g/L	0.1 mol/L	0.844 mol/L

Source: Ran et al., 2023

Experiments (at Laboratory of University of Gustave Eiffel)

Investigate:

☞ Damage pattern/+leaching

☞ Effect of chlorides/diffusion

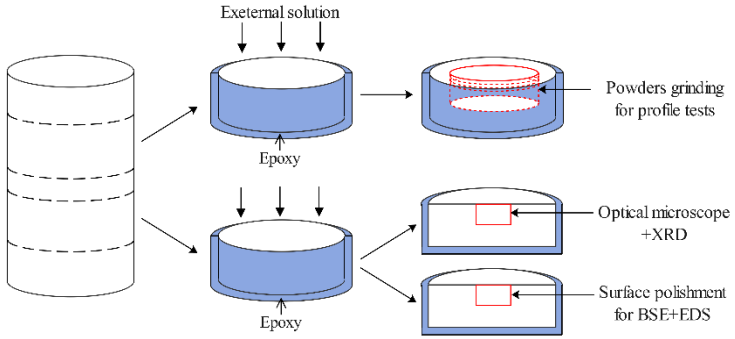

Characterization

XRD (identification of AFt)
NMR (Al phases in hydrates)
MIP (pore distribution)
DVS (vapor diffusivity)
ICP (ionic concentrations)
Potentiometer (Cl ions)

2 Sulfate attack. AFt formation

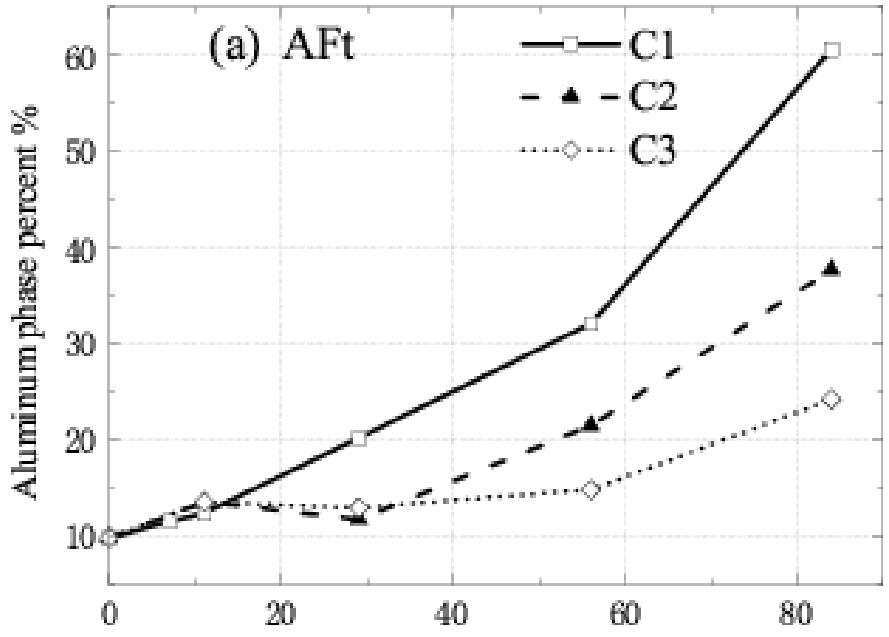

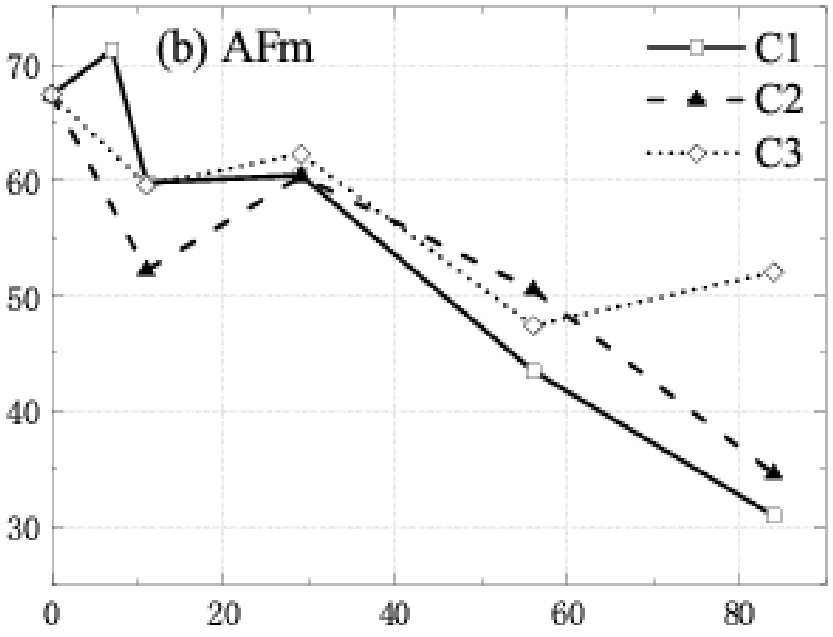

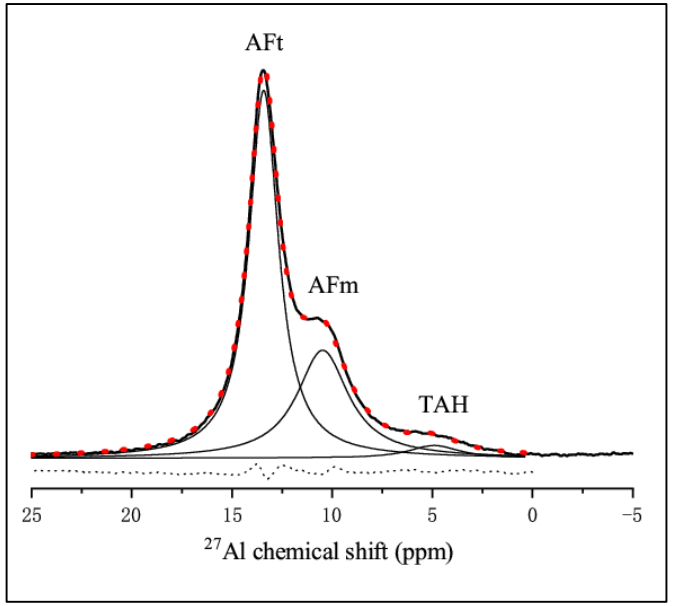

Fig. 2. Decomposition of 27Al MAS NMR spectrum of cement paste (w/c=0.55) for 84-day exposure to sodium sulfate solution of 10 g/L SO_4^{2-} , using multi-peaks fitting method in [29]. The black solid line represents the experimental spectrum, and the red dotted line is the simulated total spectrum. The solid lines with single peak stand for simulated AFt, AFm and TAH spectra respectively. The lower dotted line represents the difference between simulated and experimental spectra.

Results: Evolution of ettringite (AFt) and monosulphates (AFm) with immersion time. Note that both AFm and Friedel's salts are counted into the monosulphate phase. The inhibiting effect of chlorides on AFt formation is due to the decrease of the supersaturation of AFt in multi-species environment. The supersaturation of AFt is calculated as 5.42×10^{10} (C1), 8.37×10^{7} (C2) and 1.37×10^{7} (C3).

2 Sulfate attack. Porosity

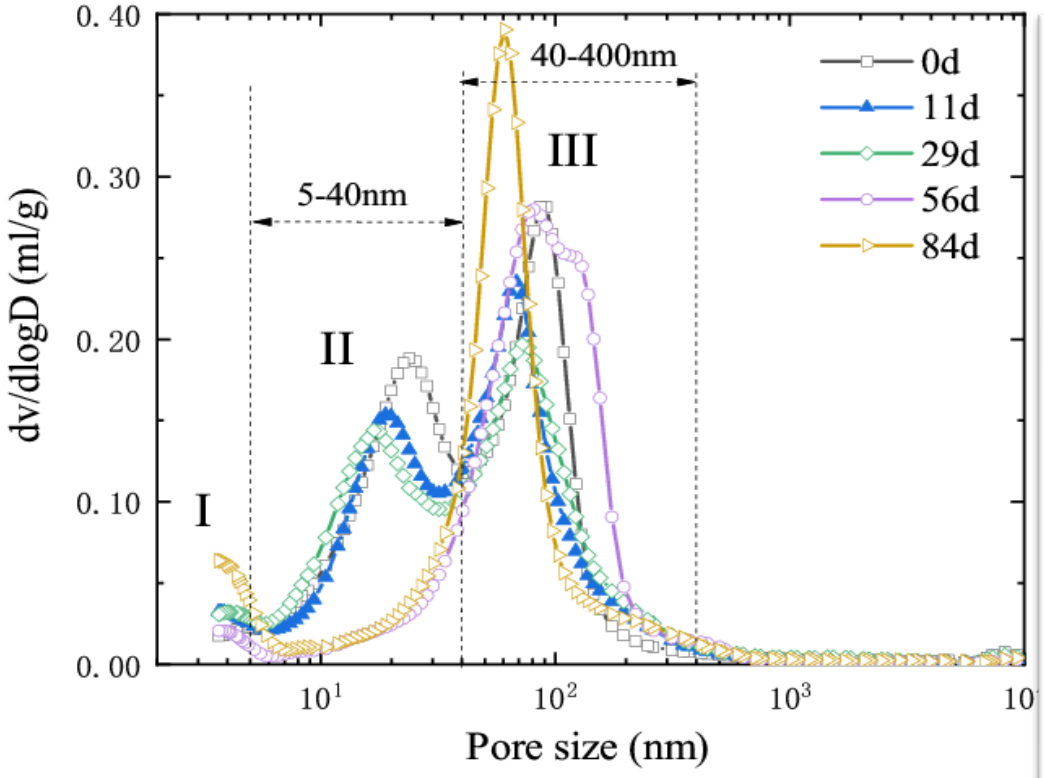

Observation (C1): the total porosity is decreasing globally, the nanopores (<5nm) increases, the micropores (5-40nm) decreases, the capillary pores (40-100nm) increase and the large capillary pores (>100nm) remain relatively stable.

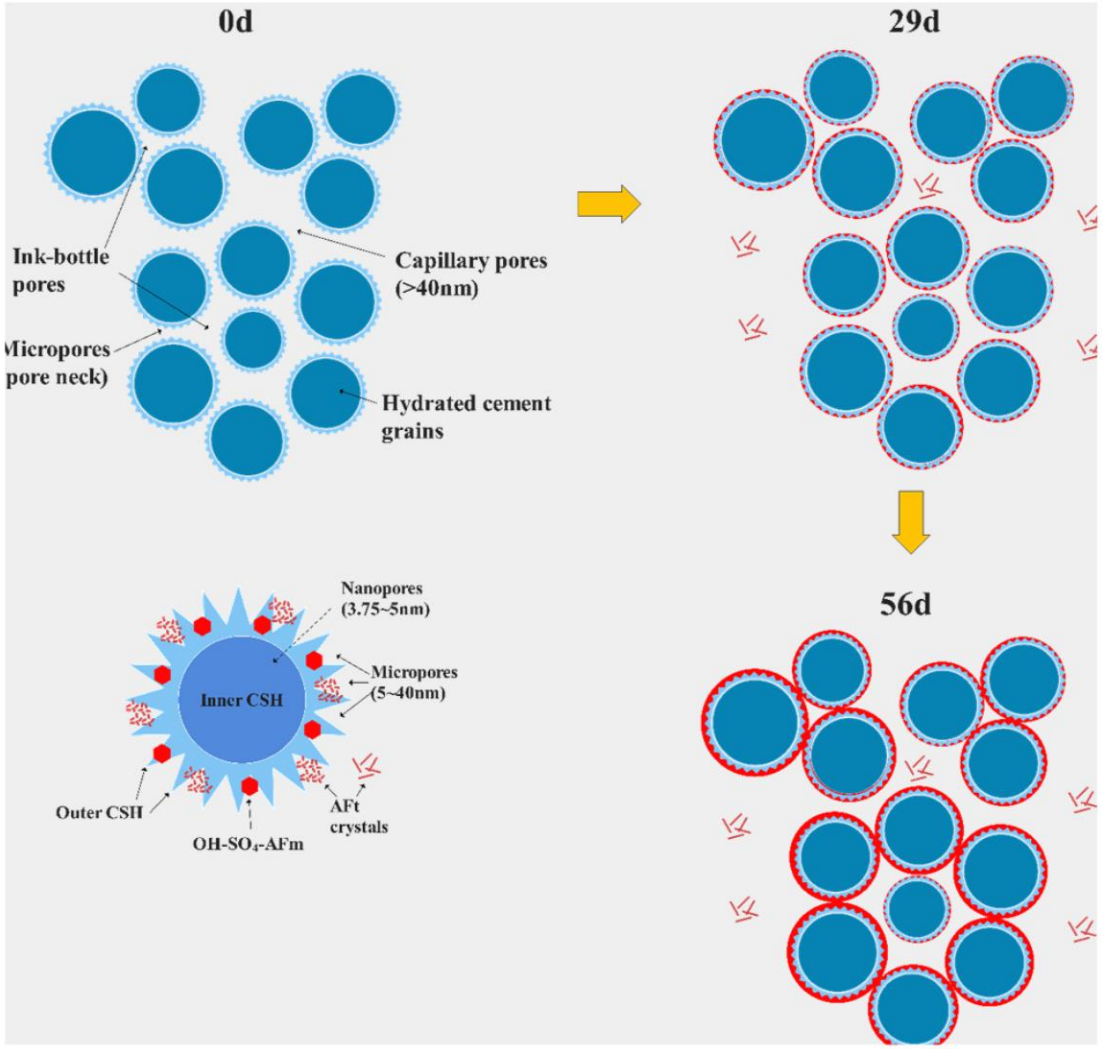

Nanopores (<5nm) ↗
The extraction of Ca^{2+} from inner CSH to outer CSH.

Micropores (5-40nm) ↘
Formation of AFt in outer CSH and its filling effect, and the blockage of new inter-granular space.

Capillary pores (40-100nm) ↗
Consumption of AFm, CH and formation of AFt, global increase

Large cap. pores (>100nm) →
Multi-factors interplaying

2 Sulfate attack. Diffusivity

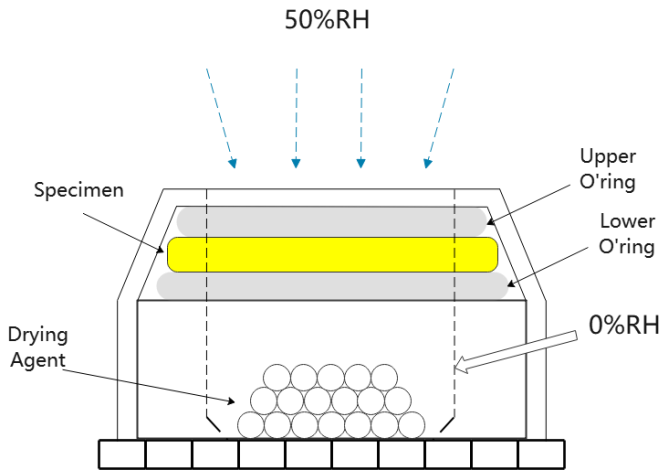

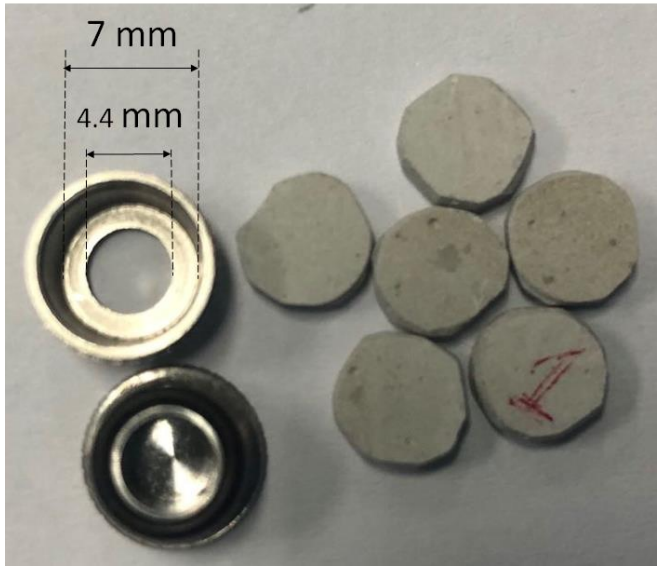

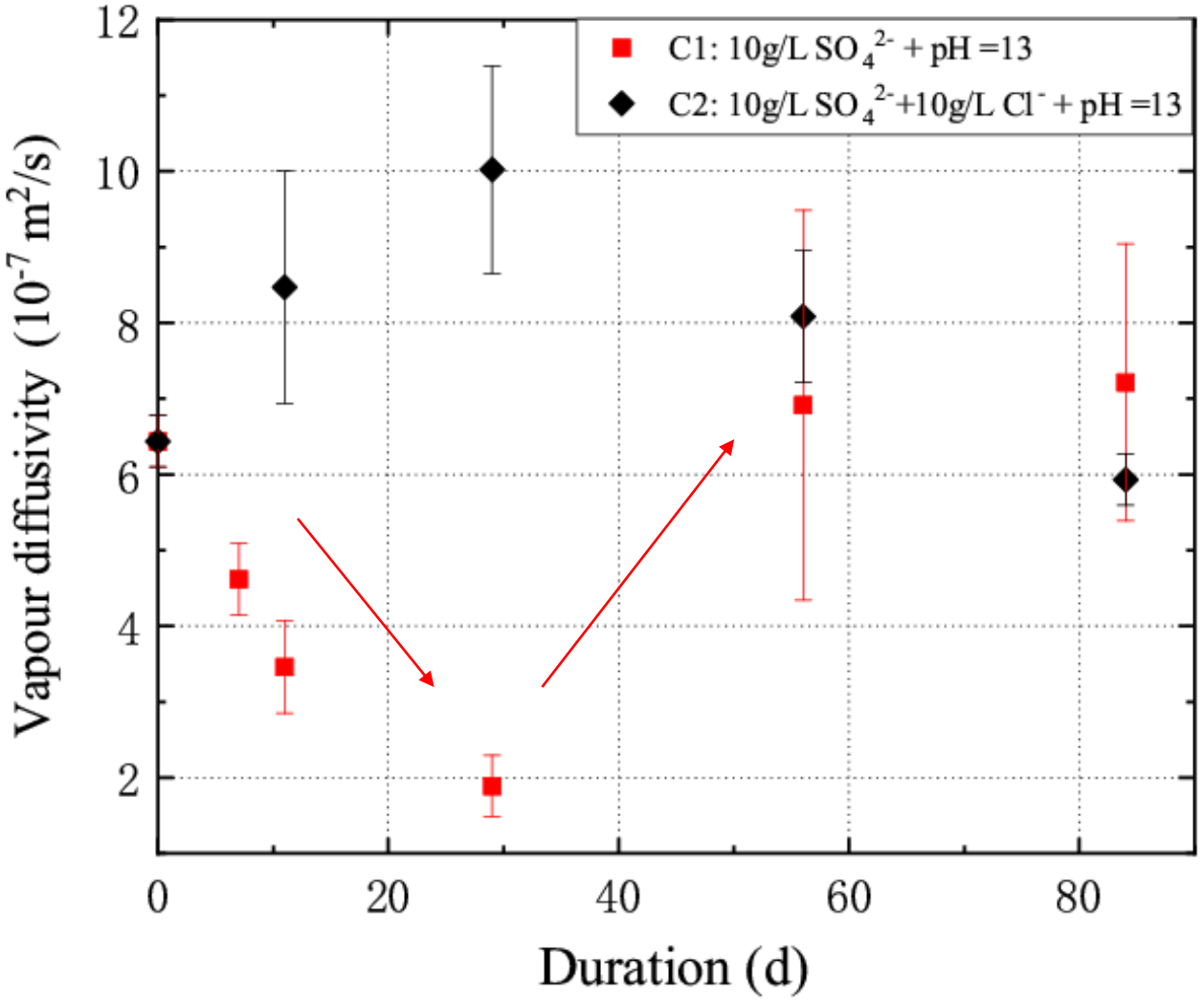

$CaCl_2$ salt: nearly 0%RH created.

Results:
Measurement of the vapor diffusivity (under 50%RH gradient). The vapor diffusivity reflects the pore space change and cracking associated with the AFt formation.

2 Sulfate attack. Expansion

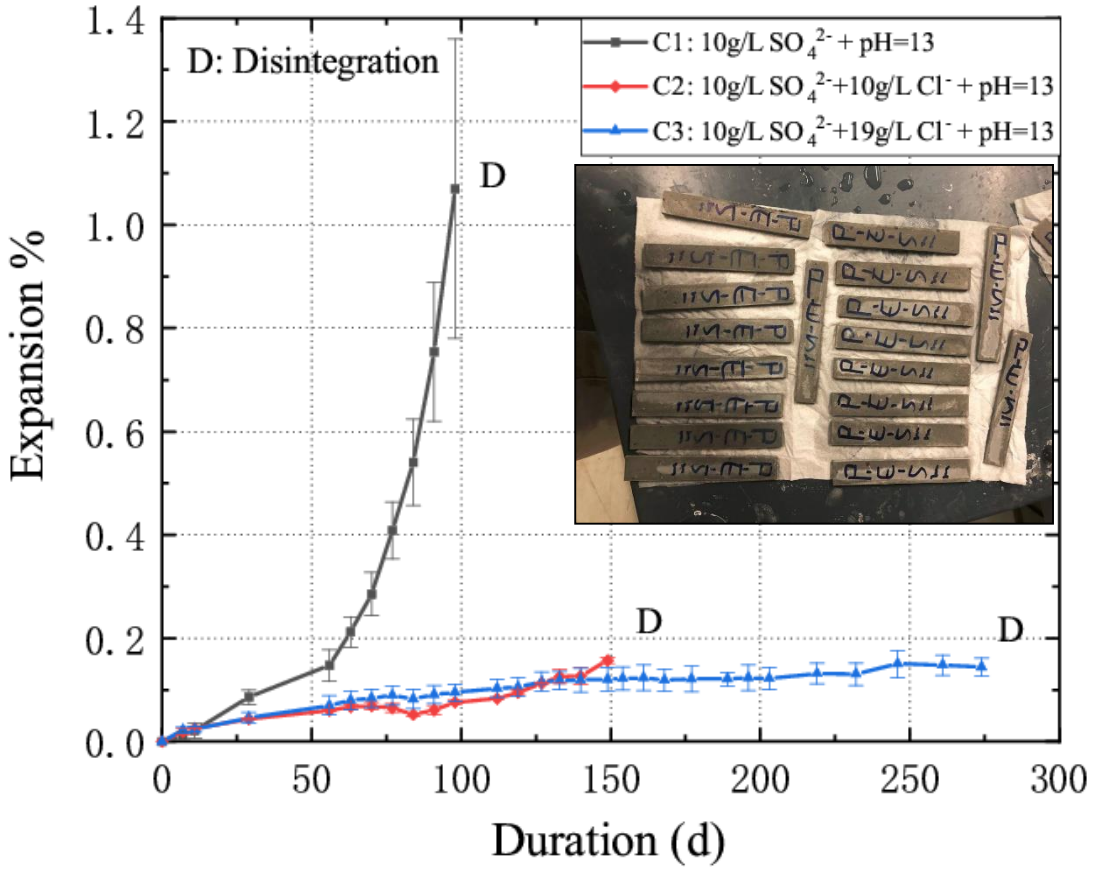

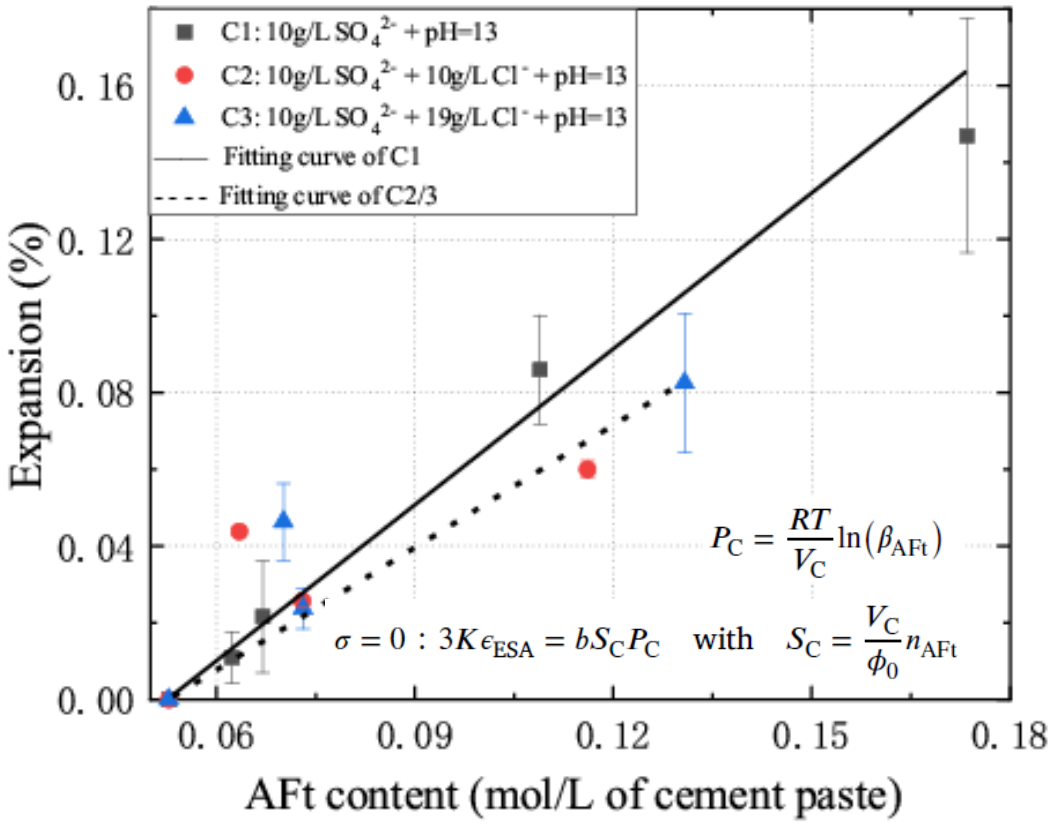

Results: Expansion of cement paste specimens presents different patterns for different sulphate exposures. Under pure sulphates, the expansion is due to AFt crystallization in pores while the expansion is largely depressed with presence of chlorides.

Results: Linear expansion of each specimen is linearly related to the AFt formation quantity. Poroelastic evaluation gives very close prediction: the slops are 8.94×10^{-6} (C1), 6.60×10^{-6} (C2) and 6.01×10^{-6} (C3). Compared to the measured slopes, 13.54×10^{-6}(C1), 10.90×10^{-6} (C2/C3).

2 Sulfate attack. Overview

Overview of evolution of properties and expansion with time for Specimen C1

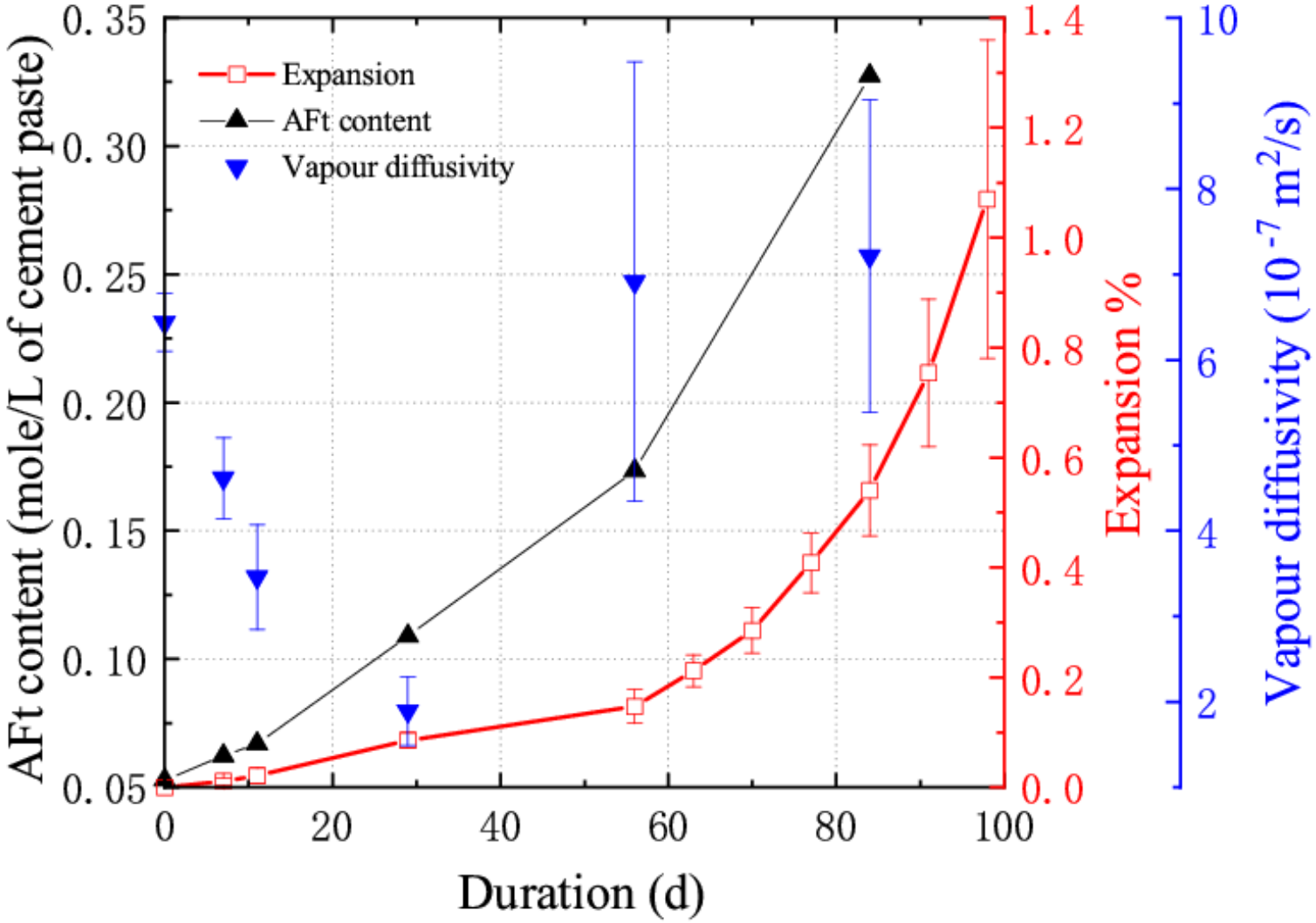

☞ Ran B., Omikrine-Metalssi O., Fen-Chong T., Dangla P., Li K.F. Pore crystallization and expansion of cement pastes in sulfate solutions with and without chlorides, Cement and Concrete Research, 166 (2023) 107099

2 Sulfate attack. Leaching/Cl

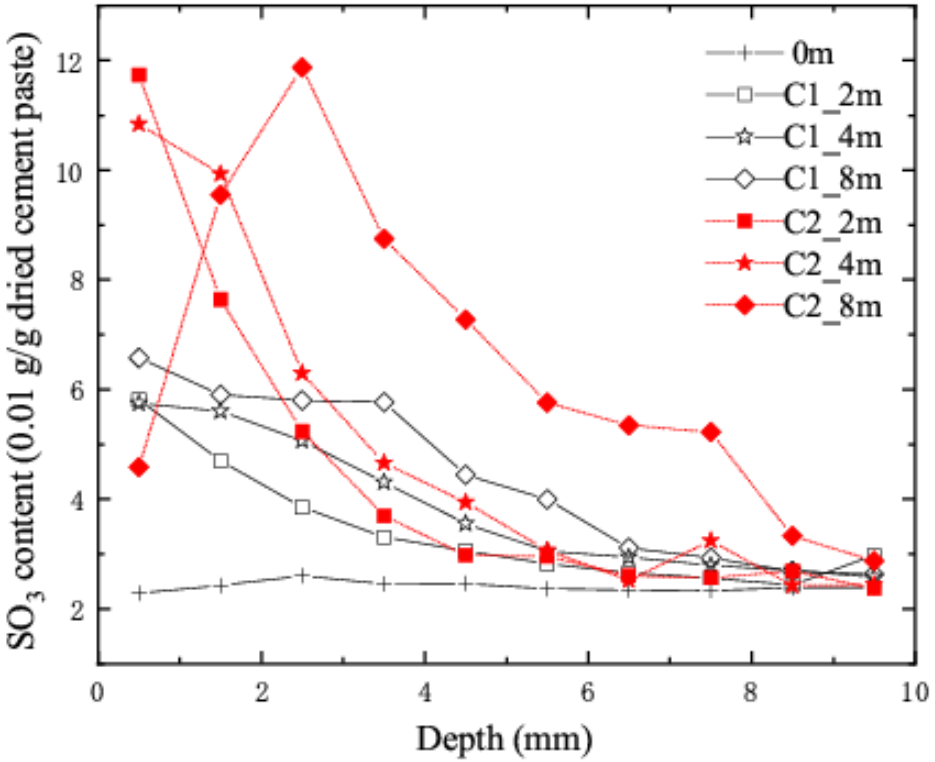

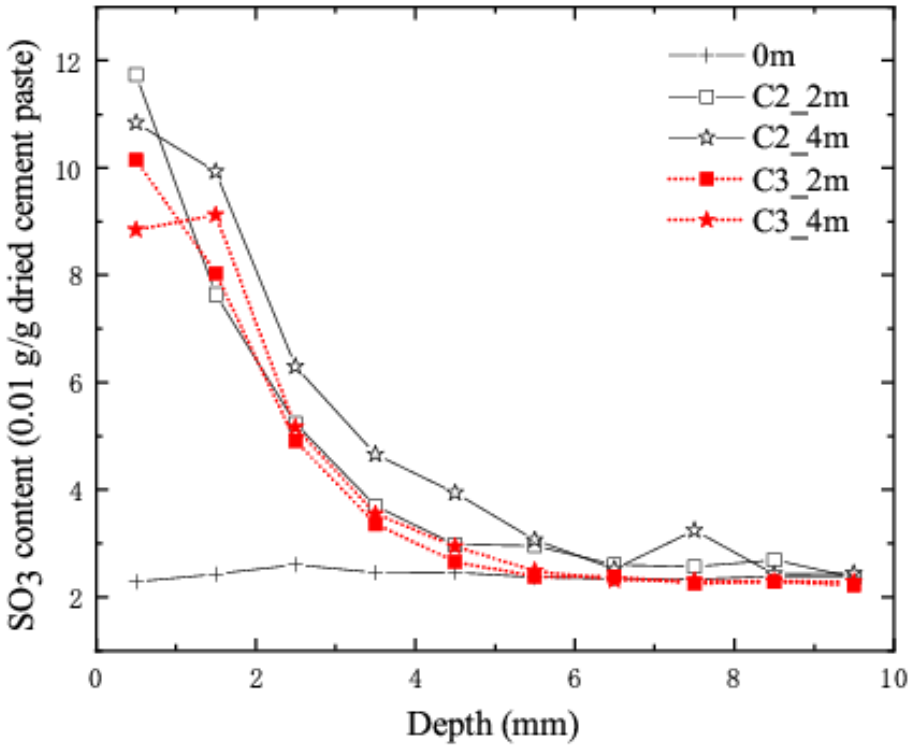

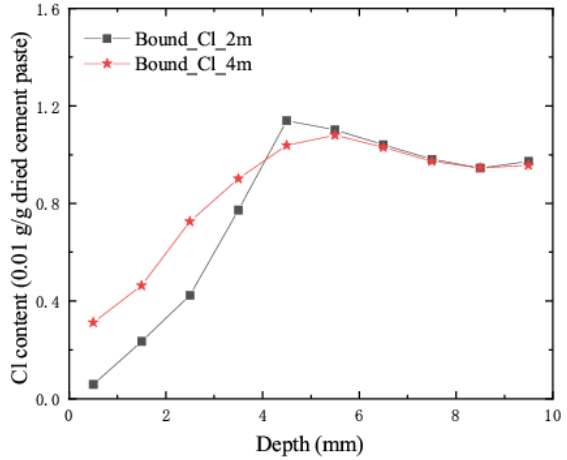

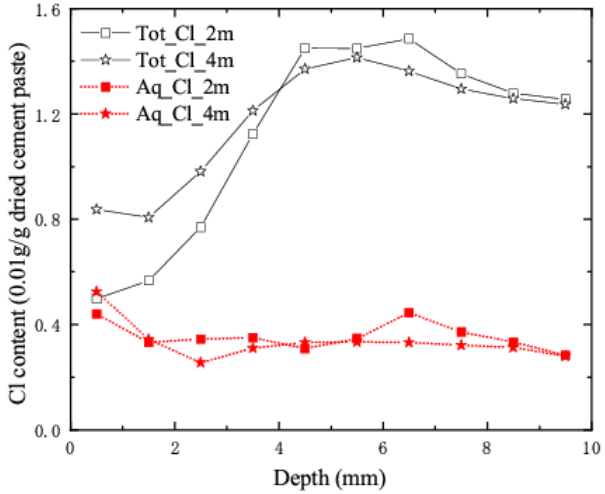

Profiles from Disc specimens (∅100mm*50mm):
C1 (10g/L sulfate, pH=13): Sulfate reaction <u>without leaching</u>
C2' (10g/L sulfate, pH=7) : Sulfate reaction <u>with leaching</u>
C3' (10g/L sulfate, 19g/L Cl, pH=7) : Sulfate reaction <u>with leaching + chlorides</u>

☞ Ran B., Omikrine-Metalssi O., Fen-Chong T., Dangla P., Li K.F. Impact of leaching and chlorides on sulfate attack for cement paste, Construction and Building Materials, 376 (2023) 130881

2 Sulfate attack. Damage

C1 Sulfate without leaching	C2' Sulfate with leaching	C3' Sulfate with leaching+Cl

60d

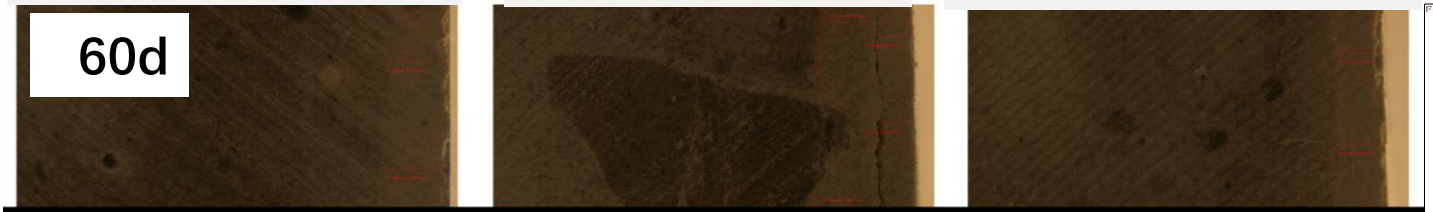

120d

240d

Damage pattern:
C1 (surface cracking)
C2, C3 (spalling).

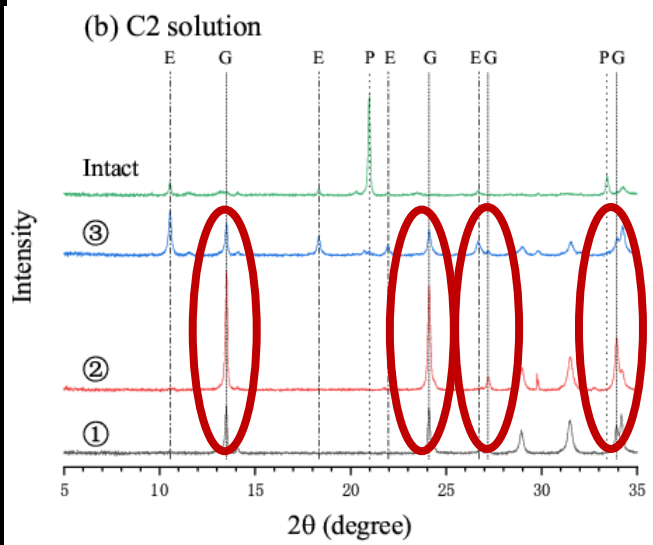

Product analysis:
Notable quantity of gypsum is detected for C2' and C3' specimens after exposure, not for C1.

2 Sulfate attack. Gypsum

Gypsum supersaturation

$$\beta_{gp} = \frac{a_{Ca^{2+}} a_{SO_4^{2-}}}{K_{gp}}$$

Calcium activity

$$a_{Ca^{2+}} = \frac{K_{CH}}{\gamma_{\pm 1}^2 \cdot c_{OH^-}^2}$$

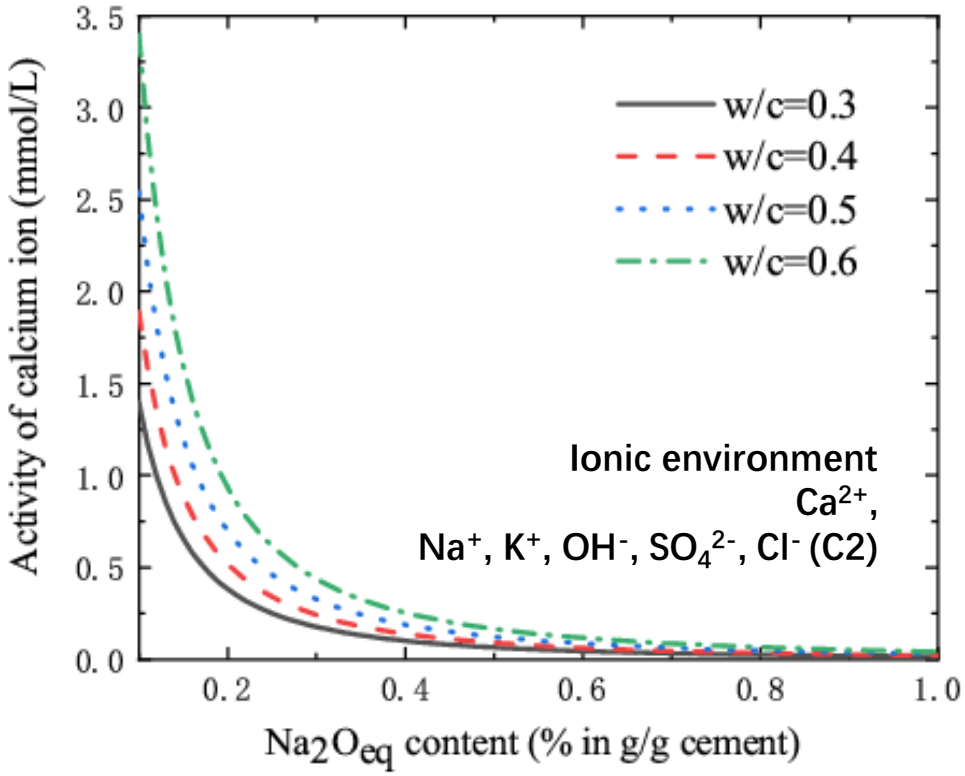

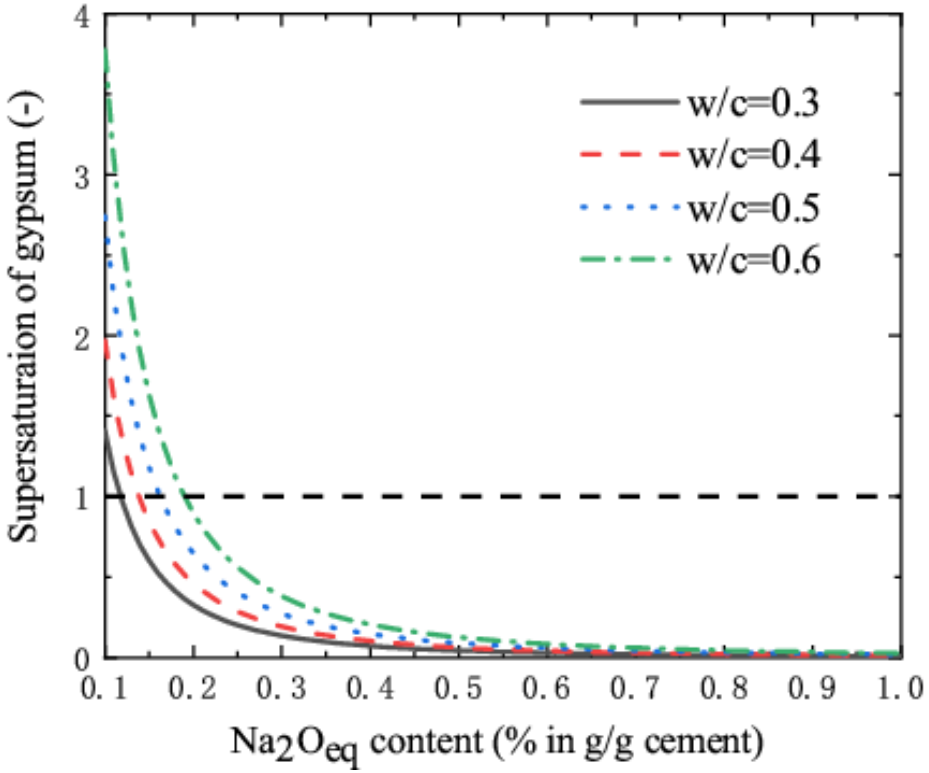

Observation: Gypsum cannot be formed in C1 solution because β_{gp} inferior to 1.0, the calcium activity is even lower in C2 solution due to the calcium leaching. So, the gypsum cannot be formed in pores in either case. However, as the formed AFt damages the solid matrix and fracture occurs. The neutral sulfate solution comes into contact with the pore solution (calcium with higher activity) and precipitates gypsum in cracks.

2 Poromechanics. Kinetics

Crystal (AFt) growth in pores

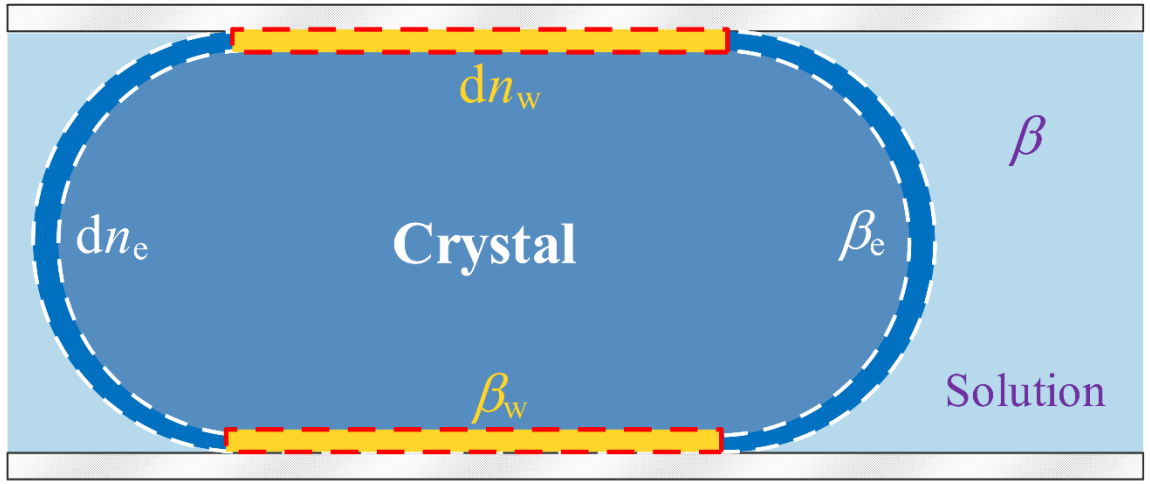

Kinetics of crystal growth

$$\frac{dn_e}{dt} = kA_e\left(\left(\frac{\beta}{\beta_e}\right)^{1/15} - 1\right)^n \quad \text{with} \quad P_C^e = \frac{RT}{V_C}\ln(\beta_e)$$

$$\frac{dn_w}{dt} = kA_w\left(\left(\frac{\beta}{\beta_w}\right)^{1/15} - 1\right)^n \quad \text{with} \quad P_C^w = \frac{RT}{V_C}\ln(\beta_w)$$

☞ Ran B., Dangla P., Omikrine-Metalssi O., Fen-Chong T., Li K.F. Pore crystallization in cementitious solids: kinetics and external constraint, in preparation

Chemical environment:

Solids: CH (Portlandite), C_4AH_{13} (OH-AFm)

Ions: Ca^{2+}, Na^+, $Al(OH)_4^-$, OH^-, SO_4^{2-}(neutrality)

Supersaturations CH, OH-AFm

$$\beta_{C_4AH_{13}} = \left(a_{Ca^{2+}}\right)^4\left(a_{Al(OH)_4^-}\right)^2\left(a_{OH^-}\right)^6 / K_{C_4AH_{13}}$$

$$\beta_{CH} = a_{Ca^{2+}}\left(a_{OH^-}\right)^2 / K_{CH}$$

Dissolution limits CH, OH-AFm

$$n_{CH} \geq 0; \quad \beta_{CH} \leq 1; \quad n_{CH}\left(\beta_{CH} - 1\right) = 0$$

$$n_{C_4AH_{13}} \geq 0; \quad \beta_{C_4AH_{13}} \leq 1; \quad n_{C_4AH_{13}}\left(\beta_{C_4AH_{13}} - 1\right) = 0$$

Supersaturation AFt

$$\beta = \left(a_{Ca^{2+}}\right)^6\left(a_{OH^-}\right)^4\left(a_{Al(OH)_4^-}\right)^2\left(a_{SO_4^{2-}}\right)^3 / K_{AFt}$$

2 Poromechanics. Deformation

Deformation by pore crystallization

$$\sigma = K\epsilon - bS_C P_C^W$$
$$\varphi_C = bS_C\epsilon + P_C^W / N_{CC}$$

$$\phi_0 S_C = V_C n_e$$
$$\varphi_C = V_C n_w$$

Incompressible crystal, deformable matrix

$$\frac{1}{N_{CC}} = \frac{b - \phi_0}{K}(S_C - bS_C^2)$$

Crystallization invades larger pores first then smaller ones, observing

$$A_w = S_C \cdot < 2\phi_0/r >= a_w S_C$$
$$A_e = \text{constant}$$

Elastic phase

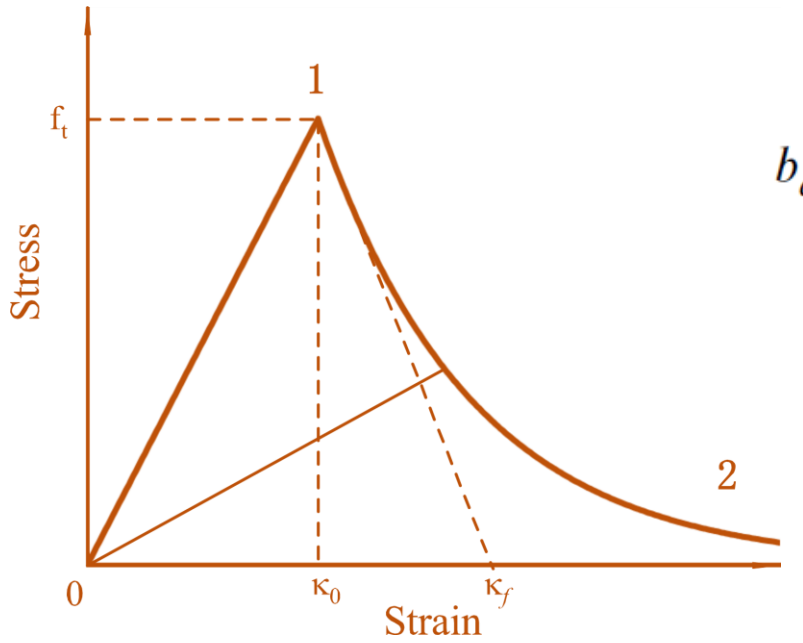

$$K_d = (1-d)K,$$
$$b_d = b + (1-b)d$$

$$d = \begin{cases} 0 & \text{if } \epsilon \le \epsilon_0 \\ 1 - \frac{\epsilon_0}{\epsilon}\exp\left(-\frac{\epsilon - \epsilon_0}{\epsilon_f}\right) & \text{if } \epsilon > \epsilon_0 \end{cases}$$

☞ Jirásek M, Patzák B. Consistent tangent stiffness for nonlocal damage models. Computers & Structures, 2002.

Damage phase

2 Poromechanics. Validation (1)

Validation by own data (C1, C2, C3 solutions, 2-2.5mm thickness cement paste)

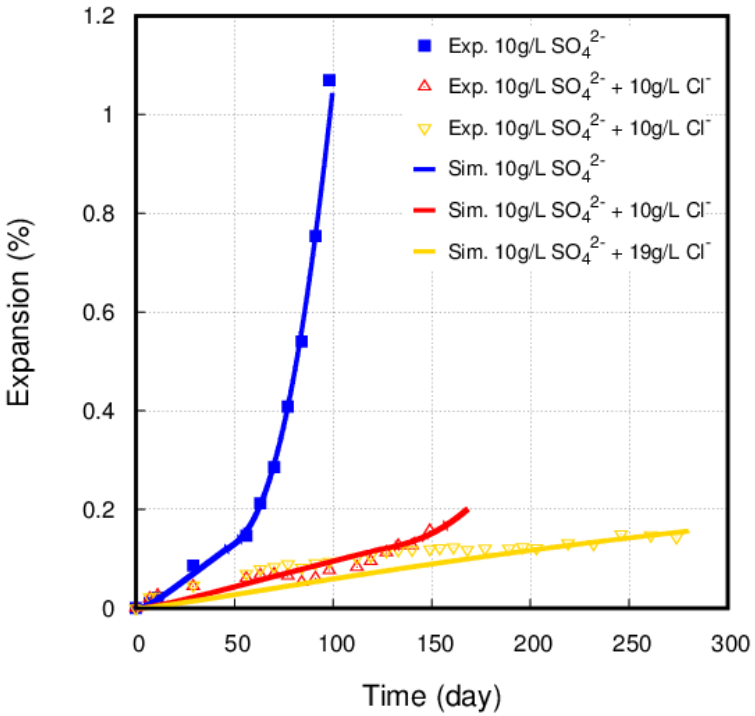

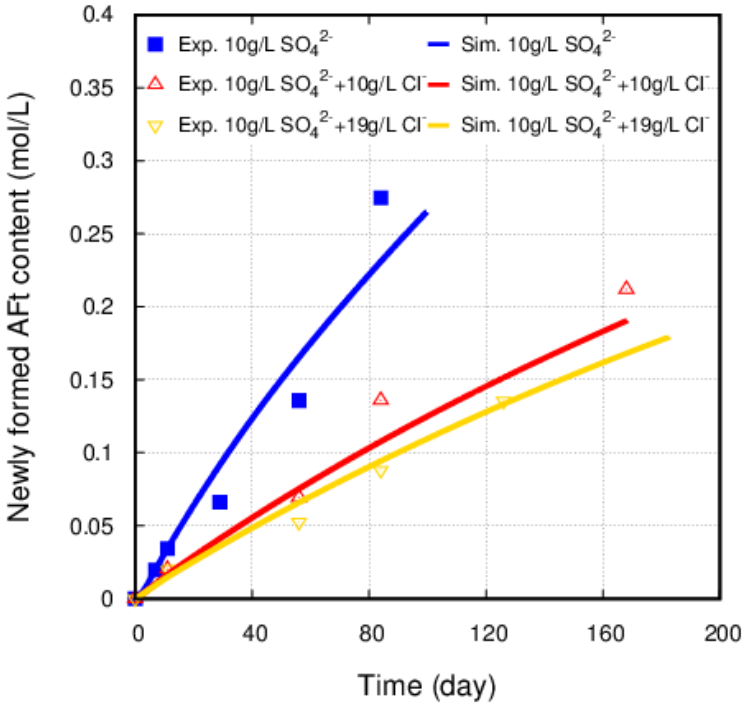

Consider chlorides in ionic environment

$$\beta_{FS} = (a_{Ca^{2+}})^4 \left(a_{Al(OH)_4^-}\right)^2 (a_{Cl^-})^2 (a_{OH^-})^4 / K_{FS} = 1$$

$$2c_{Ca^{2+}} + c_{Na^+} = 2c_{SO_4^{2-}} + c_{Al(OH)_4^-} + c_{OH^-} + c_{Cl^-}$$

K_e=2.5 10^{-9} 1/s, K_w=2.5 10^{-10} 1/s, n=1.5 (volume diffusion/integration)

2 Poromechanics. Validation (2)

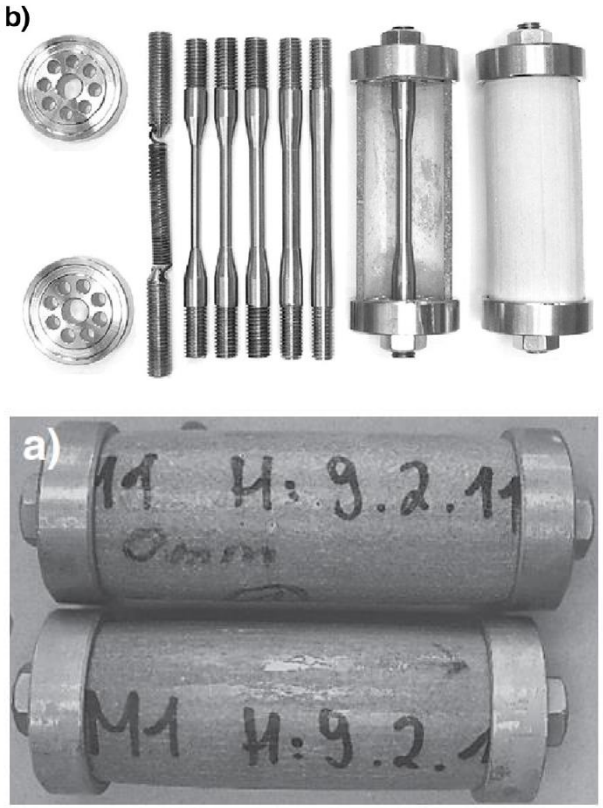

Source: Figure 1 and Figure 4 in: W. Müllauer, R. E. Beddoe, D. Heinz, Sulfate attack expansion mechanisms, Cement and Concrete Research 52 (2013) 208–215.

Validation by mortar cylinder (Mullauer et al. 2013)

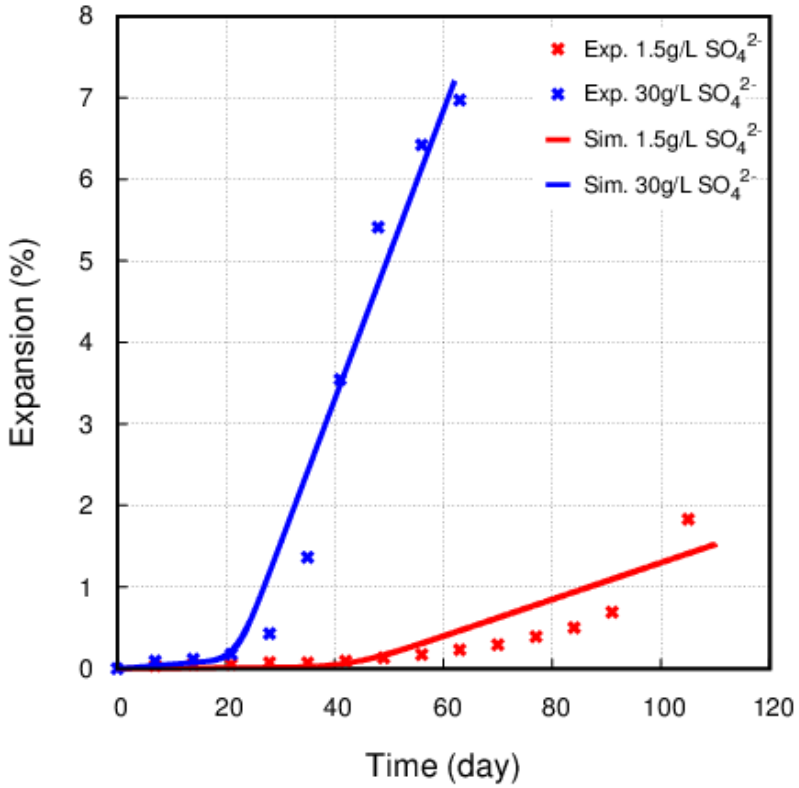

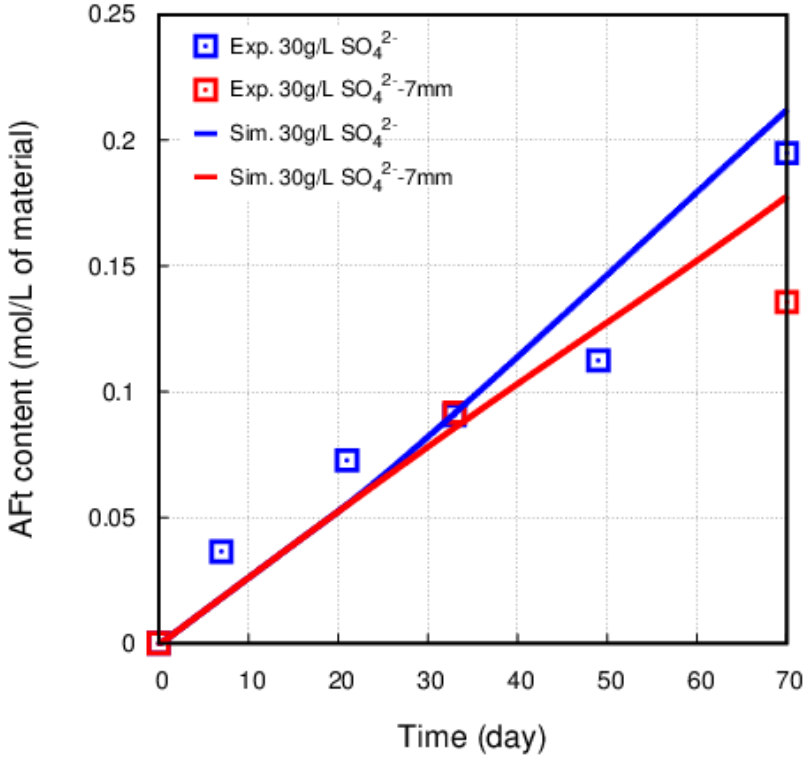

Sulfate concentration 1.5g/L, 30g/L, with/without constraint

K_e=1.2 10^{-9} 1/s, K_w=2.5 10^{-10} 1/s, n= 1.5

Constraint modulus: 80.9 10^6 N/m

2 Poromechanics. Role of stress

Role of stress : Chemo-mechanical coupling

$$\frac{d\varphi_C}{dt} = K_w S_C \left(\left(\frac{\beta}{\beta_w} \right)^{1/15} - 1 \right)^n$$

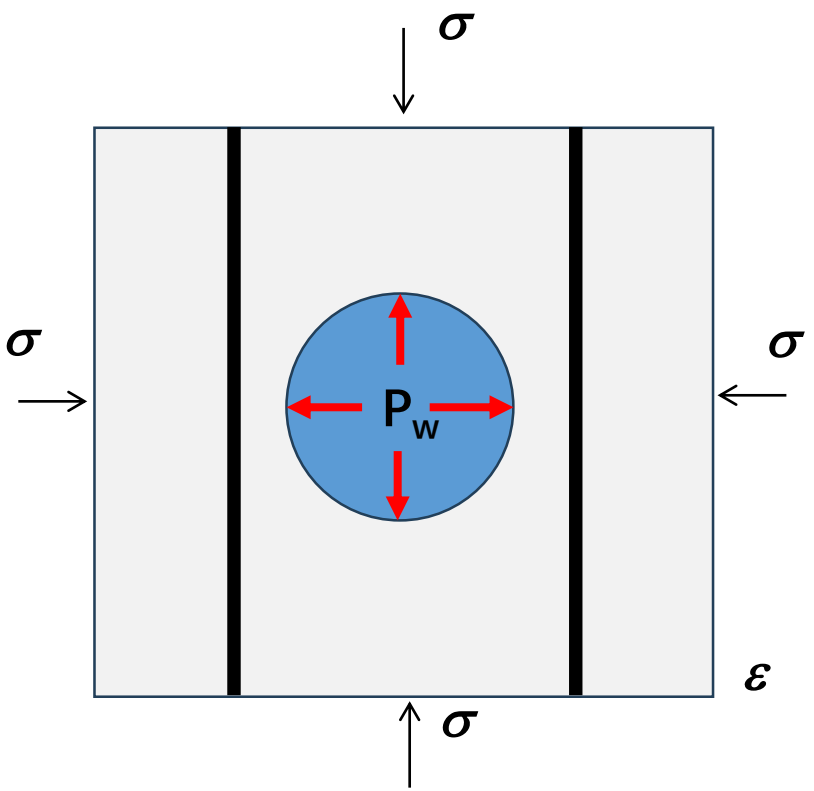

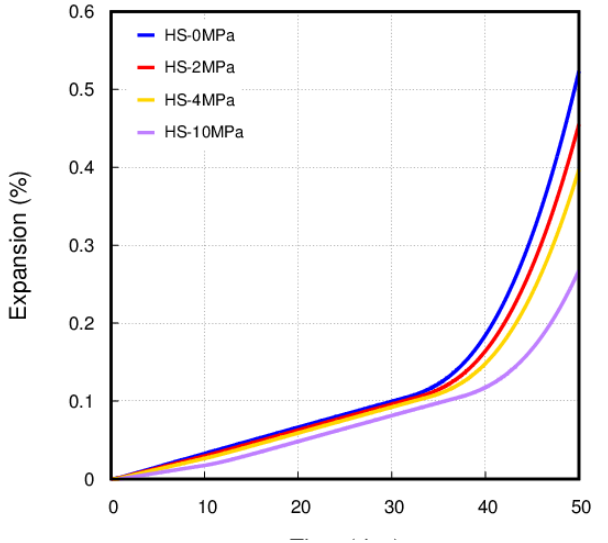

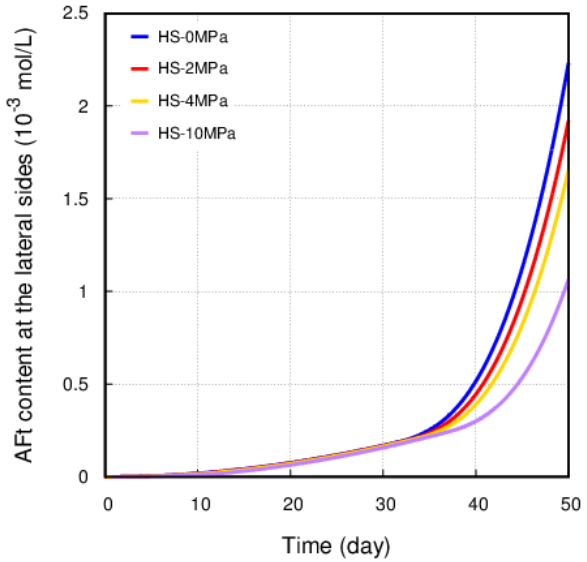

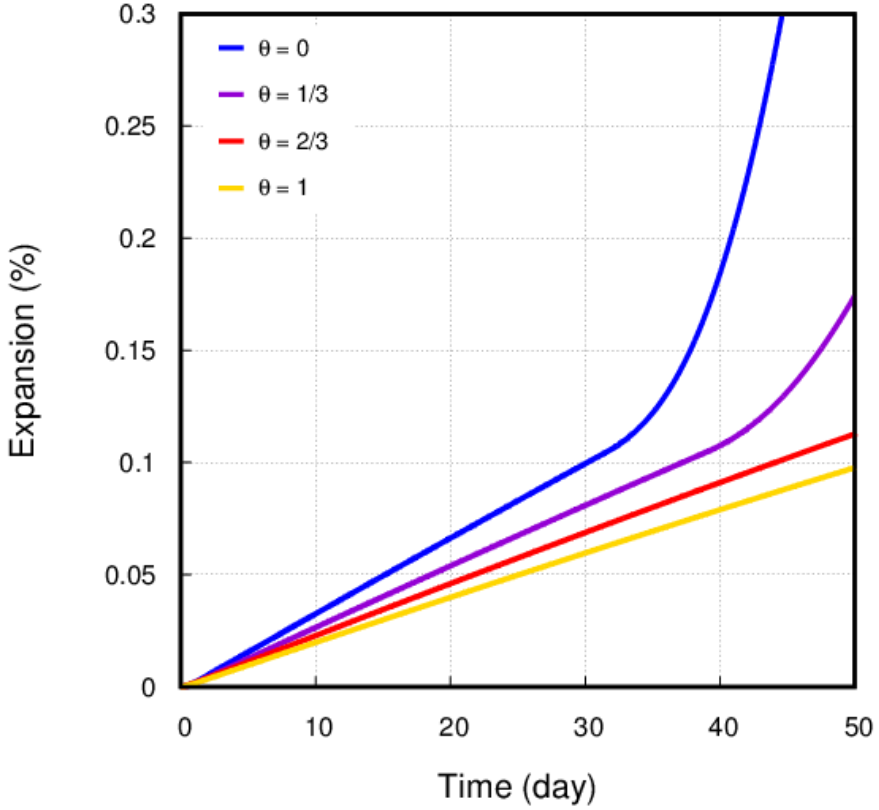

Plain strain analysis: Uniaxial constraint by external stress (0-10MPa) (left), and internal constraint by different equivalent modulus (0-100%) (up). For regular reinforcement ratio 1-8%, the equivalent modulus is about 7-60%.

3 Model for Engineering

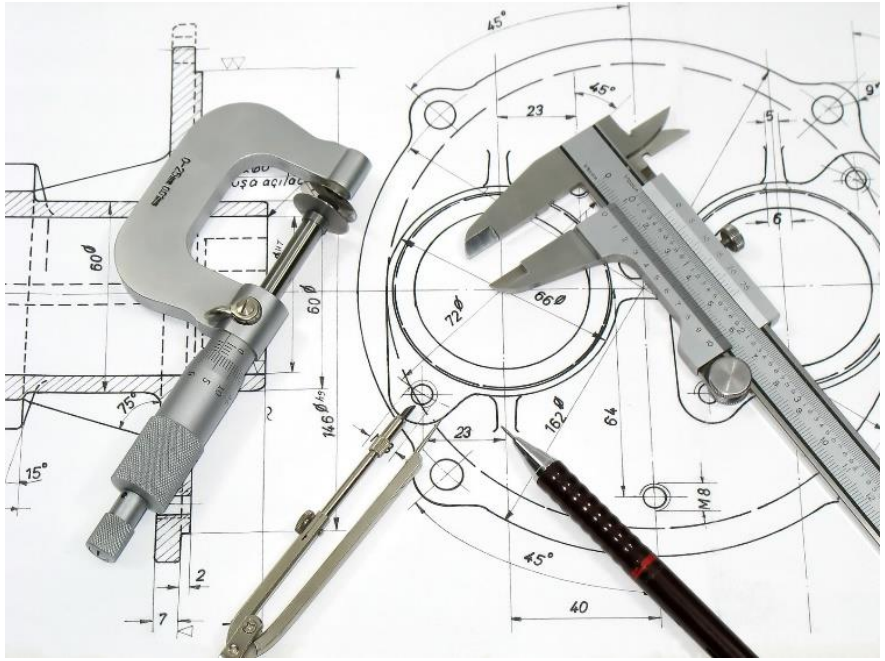

https://youthincmag.com/innovation-product-design/engineering-tools-on-technical-drawing

3 Spalling rate. Problem

Statement of Problem

Unidimensional problem of external sulfate diffusion; Simultaneous dissolution-transport of CH leaching; Concrete as totally saturated porous medium, AFt formation controlled by the supersaturation of AFt.

AFt Supersaturation

$$\beta_{AFt} = \frac{a^6_{Ca^{2+}} a^2_{Al(OH)_4^-} a^4_{OH} a^3_S}{K_{AFt}}$$

Sulphate diffusion

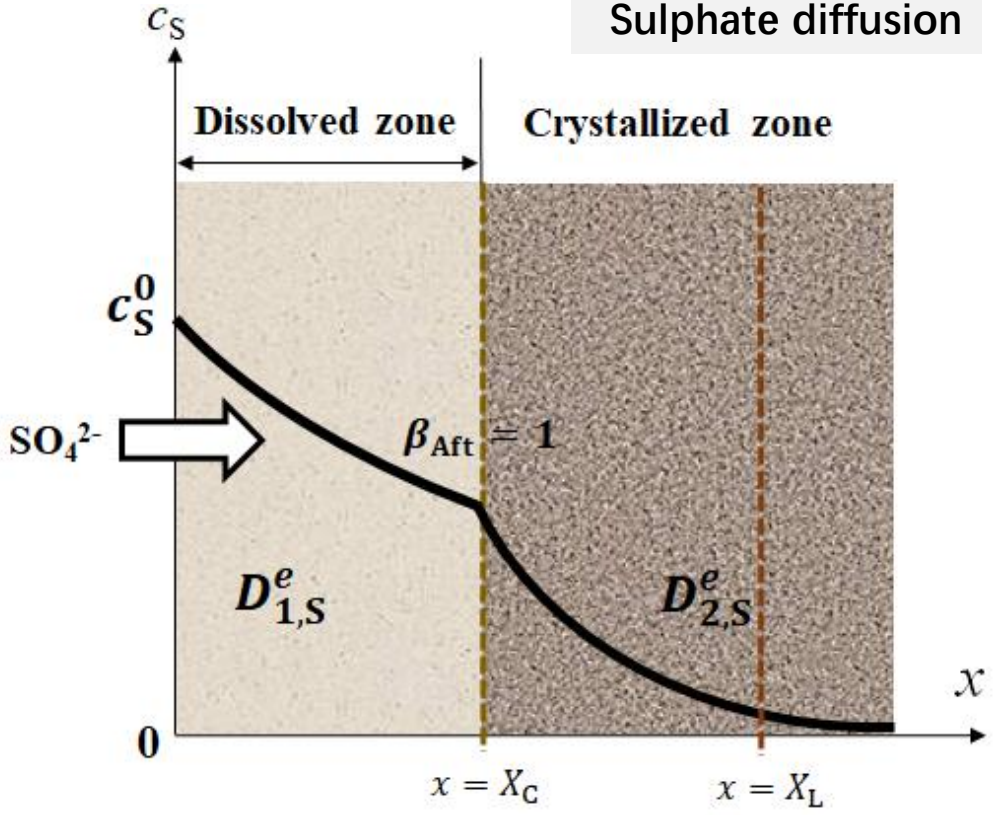

AFt formation

$$C_3AH_6 + 3Ca^{2+} + 3SO_4^{2-} + 26H_2O \rightarrow C_3A(C\bar{S})_3H_{32}$$

CH leaching

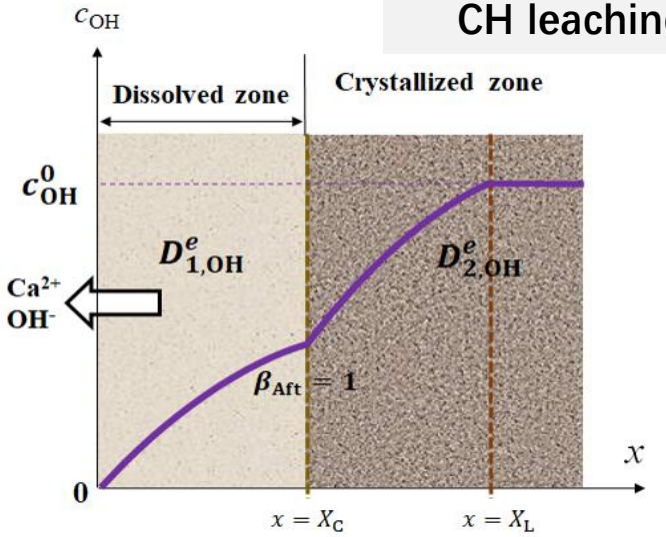

Supersaturation

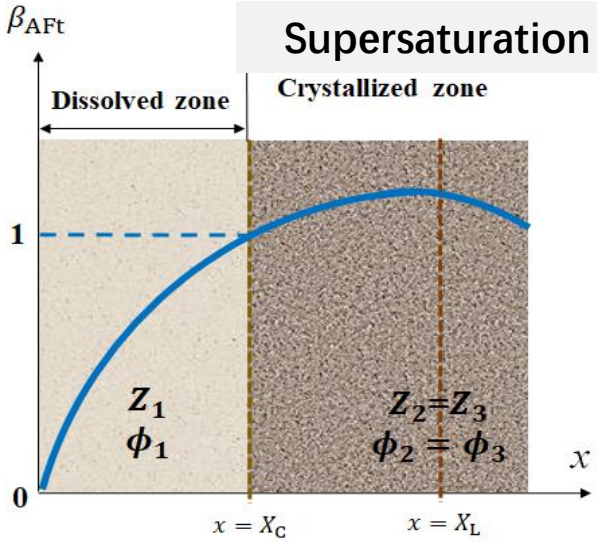

3 Spalling rate. Three zones

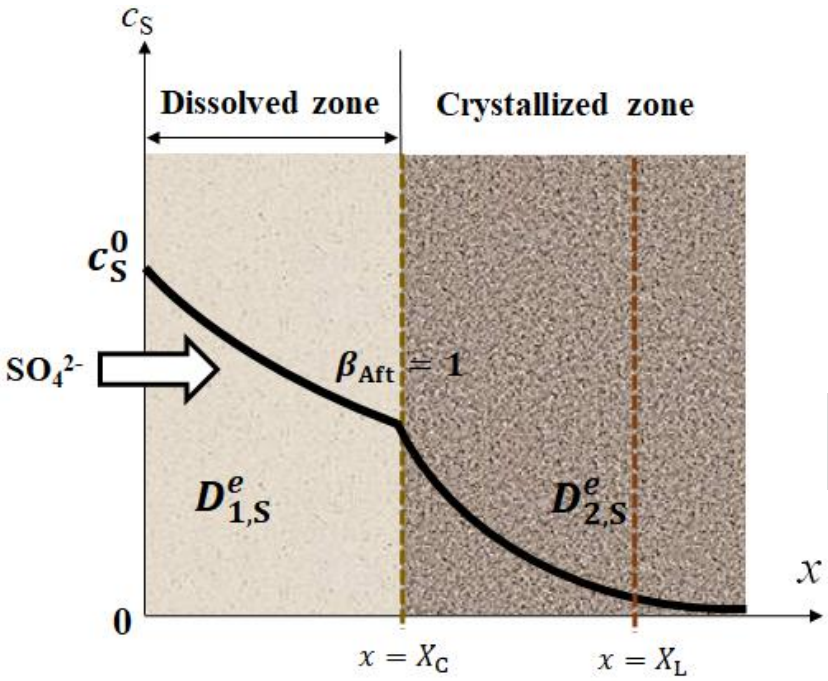

Dissolved zone (Z_1)

$$x < X_C,\ \beta_{AFt} < 1$$

Zone affected by leaching, no CH and no AFt left

Crystallized zone (Z_2)

$$X_C < x < X_L,\ \beta_{AFt} > 1$$

Zone affected by leaching, no CH left but AFt exists

Intact zone (Z_3)

$$x \geq X_L$$

Zone not affected by leaching, with CH and possibly AFt

Assumption

$$\phi_1 = \text{const}, \phi_2 = \phi_3 = \text{const}$$

$$D^e_{1,2;i} = \text{const}.$$

3 Spalling rate. Dual diffusion

Diffusion of sulphates （SO_4^{2-}）

$$\begin{cases} \dfrac{\partial c_S}{\partial t} = D_{1,S}\dfrac{\partial^2 c_S}{\partial x^2}, \quad x < X_C \quad \text{with} \quad D_{1,S} = \dfrac{D^e_{1,S}}{\phi_1 + n'_S}, \quad n'_S = 0 \\ \dfrac{\partial c_S}{\partial t} = D_{2,S}\dfrac{\partial^2 c_S}{\partial x^2}, \quad x \geq X_C \quad \text{with} \quad D_{2,S} = \dfrac{D^e_{2,S}}{\phi_2 + n'_S} \end{cases}$$

Initial and boundary conditions

$$\begin{cases} c_S(x > 0, t = 0) = 0, \; c_S(x = 0, t > 0) = c^0_S \\ c_S|_{x=X_C^-} = c_S|_{x=X_C^+}, \; D_{1,S}\dfrac{\partial c_S}{\partial x}\Big|_{x=X_C^-} = D_{2,S}\dfrac{\partial c_S}{\partial x}\Big|_{x=X_C^+} \end{cases}$$

$$n_S = \phi_2 r_S c_S n_{C_3AH_6} \; : \quad D_{2;S} = \text{const}$$

Diffusion of OH^-

$$\begin{cases} \dfrac{\partial c_{OH}}{\partial t} = D_{1,OH}\dfrac{\partial^2 c_{OH}}{\partial x^2}, & x < X_C \\ \dfrac{\partial c_{OH}}{\partial t} = D_{2,OH}\dfrac{\partial^2 c_{OH}}{\partial x^2}, & X_C \leq x < X_L \\ \dfrac{\partial c_{OH}}{\partial t} = 0, & x \geq X_L \end{cases}$$

Initial and boundary conditions

$$\begin{cases} c_{OH}(x = 0, t > 0) = 0, \quad c_{OH}(x \geq X_L) = c^0_{OH} \\ c_{OH}|_{x=X_C^-} = c_{OH}|_{x=X_C^+}, \quad D_{1,OH}\dfrac{\partial c_{OH}}{\partial x}\Big|_{x=X_C^-} = D_{2,OH}\dfrac{\partial c_{OH}}{\partial x}\Big|_{x=X_C^+} \\ n_{CH}\dfrac{dX_L}{dt} = -\phi_2 D_{2,OH}\dfrac{\partial c_{OH}}{\partial x}\Big|_{x=X_L} \end{cases}$$

3 Spalling rate. Dual MBP

Dual – Moving Boundary Problem

Moving fronts (dissolution, leaching)

$$X_C = k\sqrt{t}, \quad X_L = \kappa\sqrt{t} \quad \text{with} \quad k \le \kappa$$

Solution of kinetics coefficients

Conservation of CH across the leaching front

$$\kappa \exp\left(\frac{\kappa^2}{4D_{2,OH}}\right) = \frac{2}{\sqrt{\pi}} \frac{\phi_2 c^0_{OH}\sqrt{D_{2,OH}}}{n_{CH}} a_2(k,\kappa)$$

Supersaturation at the dissolution front

$$\left[a_1(k,\lambda)\mathrm{erf}\left(\frac{k}{2\sqrt{D_{1,OH}}}\right)\right]^{10}\left[A_3(k)\mathrm{erf}\left(\frac{k}{2\sqrt{D_{2,S}}}\right)\right]^{3} = \frac{1}{K'}$$

$$\begin{cases} \dfrac{c_S}{c^0_S} = A_1\mathrm{erfc}\left(\dfrac{x}{2\sqrt{D_{1,S}t}}\right) + A_2, & \\ \dfrac{c_{OH}}{c^0_{OH}} = a_1\mathrm{erf}\left(\dfrac{x}{2\sqrt{D_{1,OH}t}}\right), & x < k\sqrt{t} \\ \dfrac{c_S}{c^0_S} = A_3\mathrm{erfc}\left(\dfrac{x}{2\sqrt{D_{2,S}t}}\right), & \\ \dfrac{c_{OH}}{c^0_{OH}} = a_2\mathrm{erf}\left(\dfrac{x}{2\sqrt{D_{2,OH}t}}\right) + a_3, & k\sqrt{t} \le x < \kappa\sqrt{t} \\ \dfrac{c_S}{c^0_S} = A_3\mathrm{erfc}\left(\dfrac{x}{2\sqrt{D_{2,S}t}}\right), & \\ \dfrac{c_{OH}}{c^0_{OH}} = 1, & x \ge \kappa\sqrt{t} \end{cases}$$

$$A_{1,2,3} = A_{1,2,3}(k, D_{1,S}, D_{2,S})$$

$$a_{1,2,3} = a_{1,2,3}(k, \kappa, D_{1,OH}, D_{2,OH})$$

☞ Ran B., Li K.F., Fen-Chong T., Omikrine-Metalssi O., Dangla P., Spalling rate of concretes subject to combined leaching and external sulfate attack, 162 (2022) 106951

3 Spalling rate. Fracture

Poromechanics for crystallization stress

$$\sigma' = \sigma + b(S_C P_C + S_L P_L) \quad \text{and} \quad S_C + S_L = 1$$

$$P_C - P_L = \frac{RT}{V_C}\ln(\beta_{AFt})$$

$$\sigma = 0 : \sigma' = \gamma c_S \ln(\beta_{AFt}) \quad \text{with} \quad \gamma = r_S n_{C_3AH_6}\frac{\phi_2}{\phi_1} bRT$$

Elements with large surface, and the in-plan strains can be assumed to be zero

$$\epsilon_{yy,zz} = 0,$$

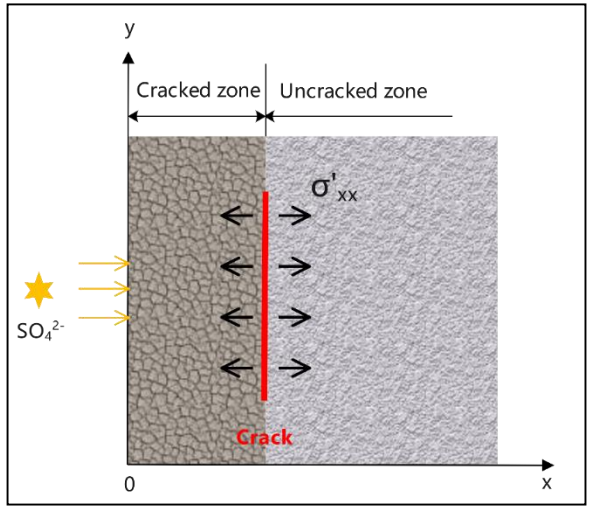

Spalling rate (elements with large surface)

$$\sigma_{xx} = 0 : \sigma'_{xx} = \gamma c_S \ln(\beta_{AFt})$$

$$\sigma'_{xx}(\eta = \eta') = \sigma_{ft} : \quad \eta' = \frac{X_{spalling}}{\sqrt{t}}$$

$$\sigma'_{xx} = \begin{cases} 0, & 0 \le \eta < k \\ \gamma c_S^0 A_3 \mathrm{erfc}\left(\frac{\eta}{2\sqrt{D_{2,S}}}\right) \ln\left\{ K'\left[a_2 \mathrm{erf}\left(\frac{\eta}{2\sqrt{D_{1,OH}}}\right) + a_3\right]^{10} \times \left[A_3 \mathrm{erfc}\left(\frac{\eta}{2\sqrt{D_{2,S}}}\right)\right]^3 \right\}, & k \le \eta < \kappa \\ \gamma c_S^0 A_3 \mathrm{erfc}\left(\frac{\eta}{2\sqrt{D_{2,S}}}\right) \ln\left\{ K'\left[A_3 \mathrm{erfc}\left(\frac{\eta}{2\sqrt{D_{2,S}}}\right)\right]^3 \right\}, & \eta \ge \kappa \end{cases}$$

3 Spalling rate. Validation

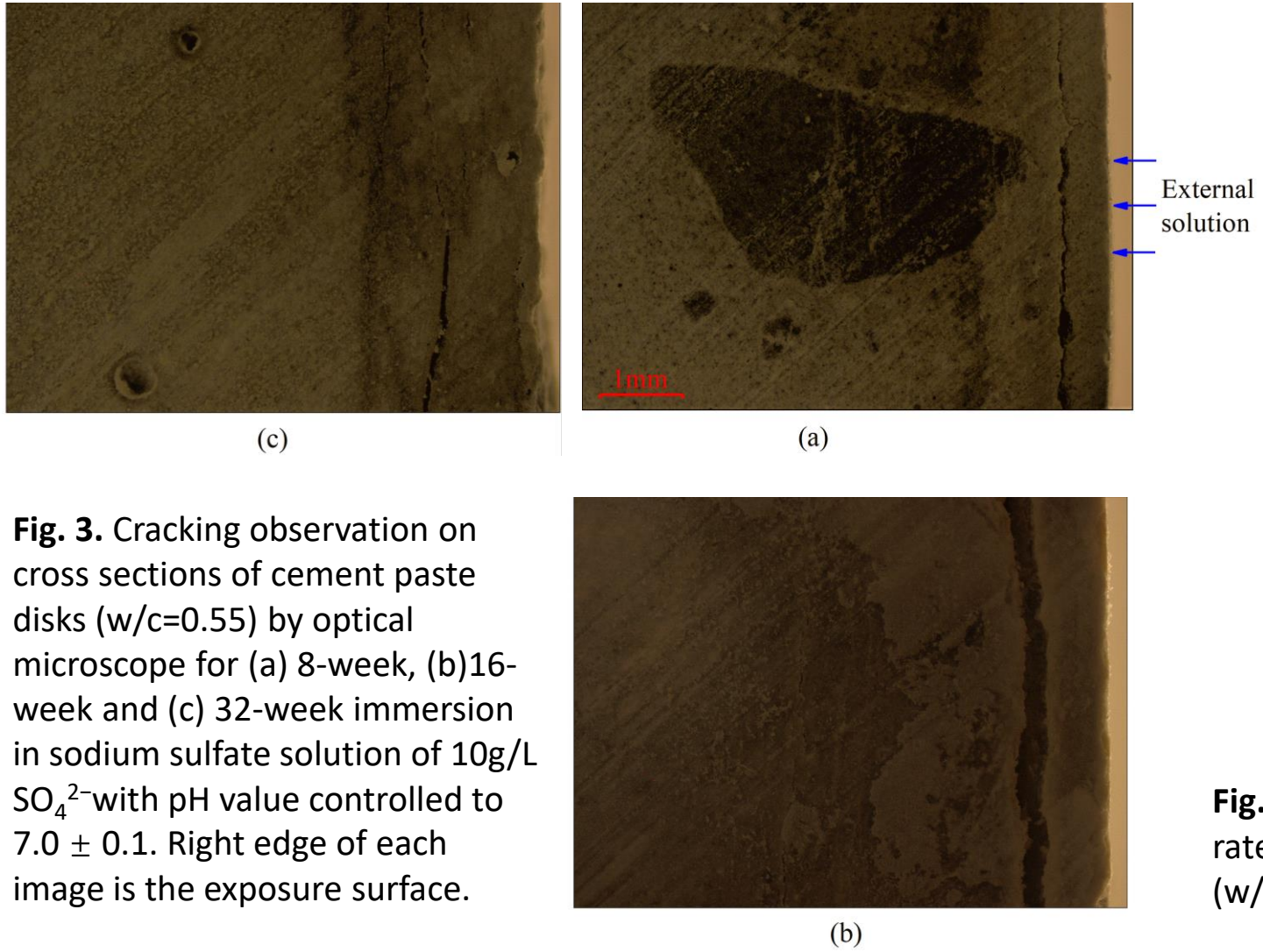

Fig. 3. Cracking observation on cross sections of cement paste disks (w/c=0.55) by optical microscope for (a) 8-week, (b)16-week and (c) 32-week immersion in sodium sulfate solution of 10g/L $SO_4^{2-}$with pH value controlled to 7.0 ± 0.1. Right edge of each image is the exposure surface.

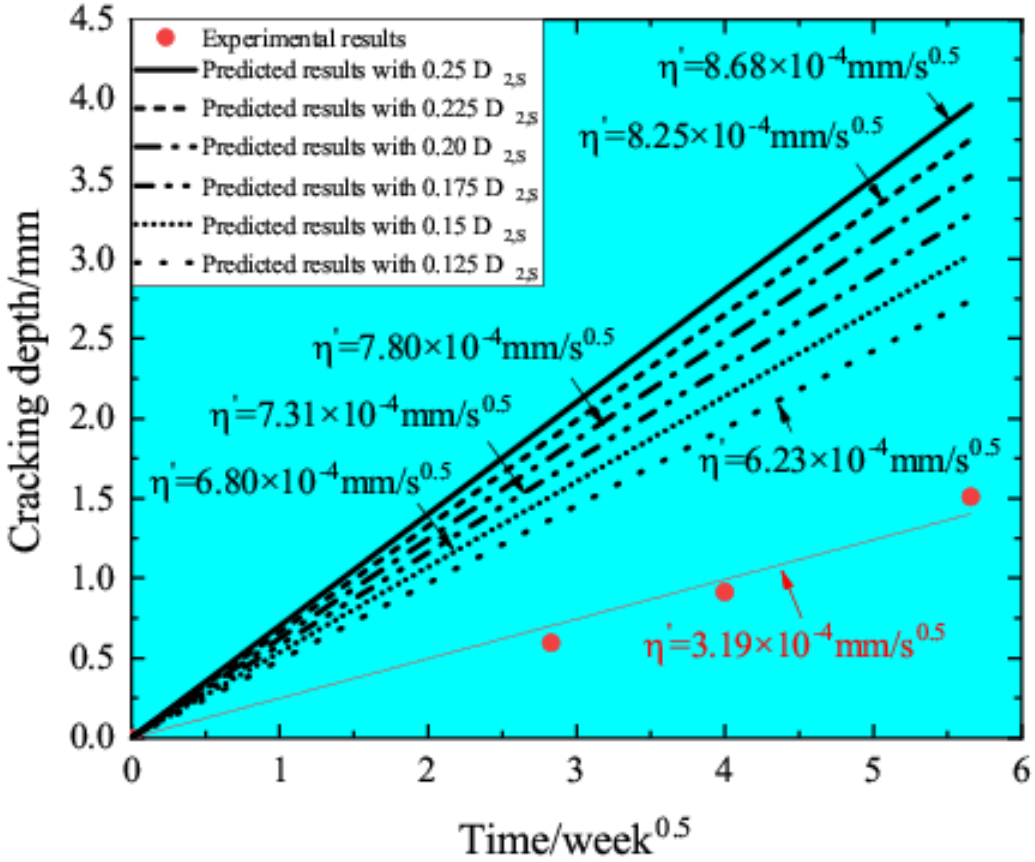

Fig. 6. Cracking depth measured in experiments and spalling rate predicted by models for disk cement paste specimens (w/c=0.55) immersed in sodium sulfate solution of 10g/L SO_4^{2-}

3 Spalling rate. Parameters

Parametric analysis (basic dimension: L/M/T)

$$\eta' = f\left(D_{1,S}, D_{2,S}; D_{1,OH}, D_{2,OH}; c_S^0, c_{OH}^0; n_{CH}, n_{C_3AH_6}; \sigma_{ft}, \frac{RT}{V_C}\right)$$

$$\eta^- = f'\left(D_S^-, k_1, \frac{D_S^-}{K_1}; c_S^-, \frac{n_{CH}}{c_{OH}^0}, \frac{n_{C_3AH_6}}{c_{OH}^0}; \frac{\sigma_{ft} V_C}{RT}\right)$$

$$\text{with} \quad \eta^- = \frac{\eta'}{2\sqrt{D_{1,OH}}}, D_S^- = \sqrt{\frac{D_{2,S}}{D_{1,OH}}}, k_1 = \sqrt{\frac{D_{2,OH}}{D_{1,OH}}},$$

$$K_1 = \sqrt{\frac{D_{1,S}}{D_{2,S}}}, c_S^- = \frac{c_S^0}{c_{OH}^0},$$

Fig. 9. Normalized spalling rate in terms of normalized boundary sulfate concentration and relative sulfate diffusivity.

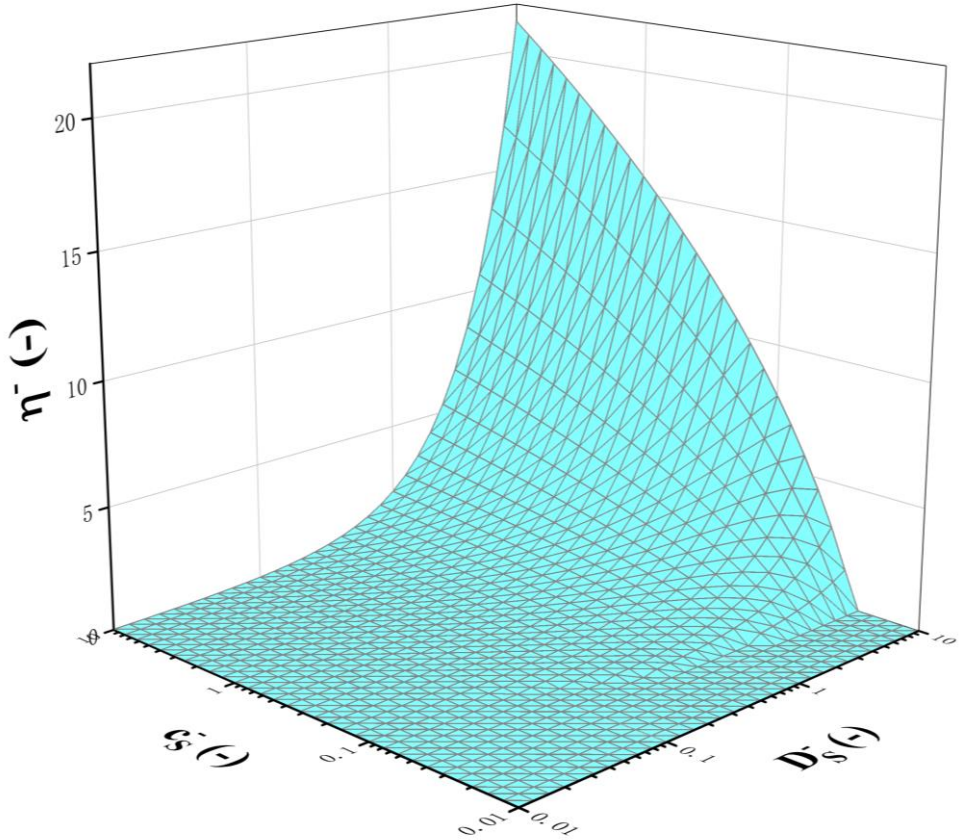

☞ Ran B., Li K.F., Fen-Chong T., Omikrine-Metalssi O., Dangla P., Spalling rate of concretes subject to combined leaching and external sulfate attack, 162 (2022) 106951

3 Spalling rate. Predictions

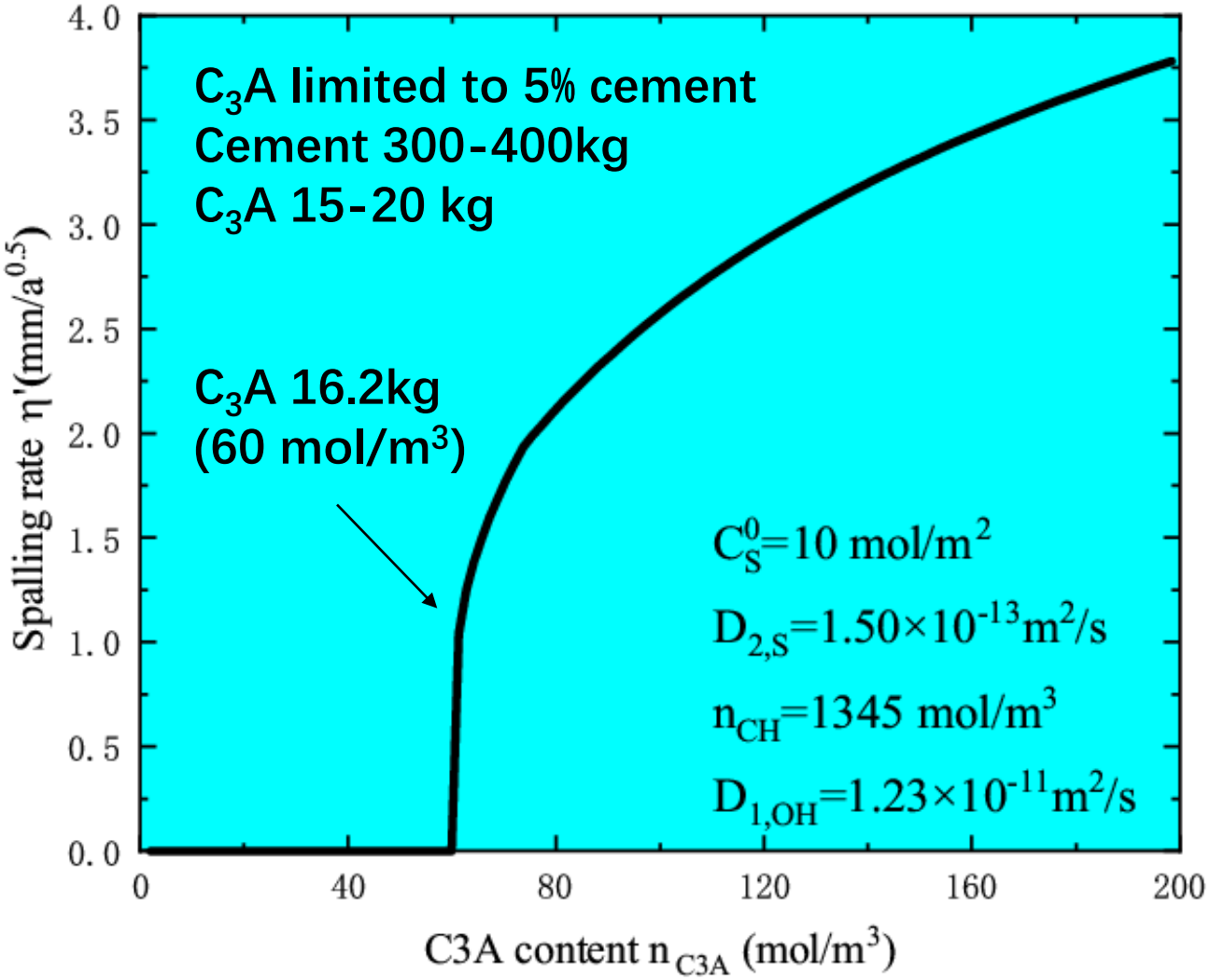

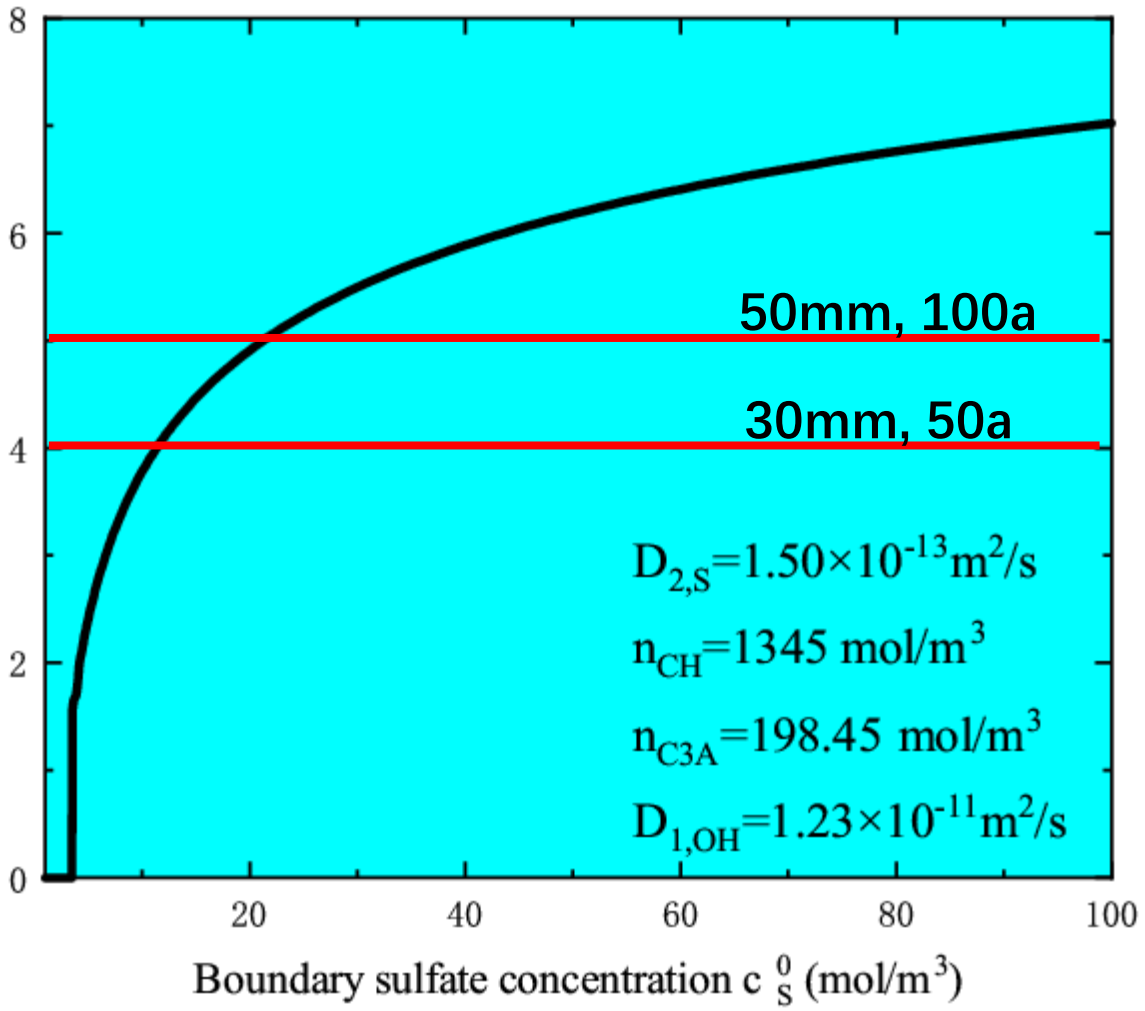

4 Concluding remarks

☞ AFt formation is strongly dependent on the multi-species pore chemistry. The crystals alter the pore structure in whole range, especially blocking the “ink-bottle” pores, the vapor diffusivity is changed through pore-filling and microcracking.

☞ The leaching accelerates the sulfate ingress and presents a damage pattern of spalling. The chlorides suppress AFt formation by decreasing AFt supersaturation. The observed gypsum is judged to form in the fracture after cracking.

☞ The poromechanical model for pore crystallization by AFt is established , considering pore chemistry, AFt supersaturation, crystallization kinetics, deformation and damage. The impact of constraint stress is underlined.

☞ Spalling rate model is established through a dual-MBP for concrete exposed to external sulfate and leaching condition (low pH value, aqueous). The model can support the specification of concrete against sulfate attack quantitatively.

Acknowledgement

Dr. Bo Ran, Chongqing University, China
Joint PhD student (2019-2022),
between Tsinghua University and Université Gustave Eiffel

Prof. Teddy Fen-Chong,
Dr. Othman Omikrine-Metalssi,
Université Gustave Eiffel, Cerema, UMR MCD

Prof. Patrick Dangla,
Navier, Ecole des Ponts, Universite Gustave Eiffel, CNRS